Supporting Information

Synergistic Conductivity Effect in a Proton Sources-Coupled Metal-Organic Framework

Xiao-Min Li,[a] Long-Zhang Dong,[a] Shun-Li Li,[a] Gang Xu,[b] Jiang Liu,[a] Feng-Ming Zhang,[a] Li-Shi Lu,[a] and Ya-Qian Lan*[a]*

a. Jiangsu Key Laboratory of Biofunctional Materials, School of Chemistry and Materials Science, Nanjing Normal University, Nanjing 210023, P. R. China

b. Fujian Institute of Research on the Struture of Matter, Chinese Academy of Sciences, Fuzhou 350002, P. R. China.

Contents

1. Experimental and synthetic details

General methods and materials: All reagents were analytical grade and used without further purification. All solutions used in experiments were prepared with Millipore water (18.25 MΩ). Chromium (III) nitrate nonahydrate ($Cr(NO_3)_2 \cdot 9H_2O$), hydrofluoric acid (HF), ethanol absolute (CH_3CH_2OH), hydrochloric acid (HCl, 36%), methanol (CH_3OH), N,N-dimethylformamide (DMF), sulfuric acid (H_2SO_4, 98%) were purchased from Sinopharm Chemical Reagent Co. Ltd. p-Phthalic acid (H_2BDC, 99%) was purchased from Aladdin. Monosodium 2-sulfoterephthalate was purchased from Tokyo Chemical Industry Co. Ltd. Chromium (VI) oxide (CrO_3, 99%) was purchased from Alfa Aesar. Powder X-Ray diffraction (PXRD) patterns were recorded on a D/max 2500VL/PC diffractometer (Japan) equipped with graphite monochromatized Cu-K_α radiation (λ = 1.54060 Å) and D8 ADVANCE X-Ray Powder Diffractometer (Germany) with Cu- K_α radiation (40KV, 40mA) over the 2θ range of 2-50°. Corresponding work voltage and current is 40 kV and 100 mA, respectively. Nitrogen adsorption-desorption isotherms were measured at 77K on a Quantachrome Instruments Autosorb AS-6B. The sample was activated under N_2 stream at 120°C for 12 hours. Energy dispersive X-ray spectroscopy (EDS) was performed with JSM-5160LV-Vantage typed energy spectrometer. Morphology analysis of the composite material was examined by a scanning electron microscope (SEM, JSM-7600F) at an acceleration voltage of 10 kV. Elemental mapping was performed with JSM-5160LV-Vantage typed energy spectrometer.

Synthesis of MIL-101 (Cr): MIL-101 (Cr) was prepared following the method described earlier.[1] $Cr(NO_3)_3 \cdot 9H_2O$ (1.99585 g) and H_2BDC (0.8281 g) were dissolved in the 35mL distilled water and then HF (0.25 mL) was added into the solution. Subsequently, the solution was transferred into a 50 mL Teflon reactor to heat at 220 °C for 8 hours. The resulting precipitate was collected by centrifugation and washed through stirring constantly with hot ethanol. After drying at 60 °C for 24 hours, the material was obtained with high yield.

Synthesis of MIL-101-SO_3H: MIL-101-SO_3H was prepared following the method described earlier.[2] Monosodium 2-sulfoterephthalic acid (3.35 g), CrO_3 (1.25 g) and concentrated aqueous hydrochloric acid (0.8 mL, 12M) were dissolved in the 25 mL distilled water. The solution was transferred into a 50 mL Teflon reactor to heat at 180 °C for six days. The resulting solid was collected by centrifugation and washed through centrifugation with distilled water and methanol. After drying in air at room temperature, the green powder was further purified in DMF at 120 °C for 24 hours and then in the mixed solution of methanol

and distilled water at 120 °C for 24 hours. After above steps, we get MIL-101-SO_3Na. The green powder was then treated in a mixed solution of 0.08 M HCl prepared with methanol and water changed once a day for three days. The final green solid was dried overnight at 120 °C in vacuum oven.

Synthesis of H_2SO_4@MIL-101 (1M, 2M, 3M): MIL-101 (0.135 g) was immersed in the diluted H_2SO_4 (1.35mL) with different concentrations of 1M, 2M and 3M respectively and then stirred 30 min at room temperature. The solution was treated by filtration and then the solid was dried at 40 °C for two hours to get H_2SO_4@MIL-101 (1M, 2M and 3M). The S/Cr ratios in H_2SO_4@MIL-101 (1M), H_2SO_4@MIL-101 (2M) and H_2SO_4@MIL-101 (3M) are 1.01, 1.59 and 2.10, respectively.

Synthesis of H_2SO_4@MIL-101-SO_3H (1M, 2M, 3M): MIL-101-SO_3H (0.135 g) was immersed in the diluted H_2SO_4 (1.35mL) with different concentrations of 1M, 2M and 3M respectively and then stirred 30 min at room temperature. The solution was treated by filtration and then the solid was dried at 40 °C for two hours to get H_2SO_4@MIL-101-SO_3H (1M, 2M and 3M). The S/Cr ratios in H_2SO_4@MIL-101-SO_3H (1M), H_2SO_4@MIL-101-SO_3H (2M) and H_2SO_4@MIL-101-SO_3H (3M) are 0.85, 0.95 and 1.31, respectively.

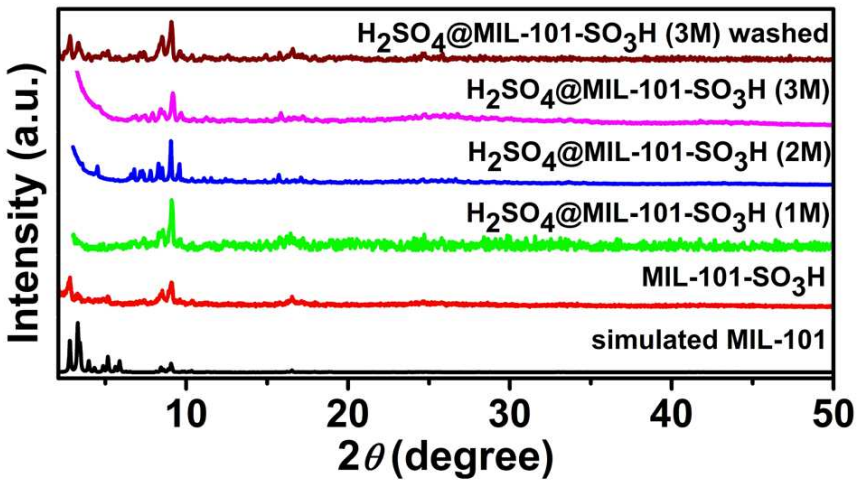

Figure S1 PXRD patterns of simulated MIL-101 (black), as-synthesized MIL-101-SO_3H (red), as-synthesized H_2SO_4@MIL-101-SO_3H (1M) (green), as-synthesized H_2SO_4@MIL-101-SO_3H (2M) (blue), as-synthesized H_2SO_4@MIL-101-SO_3H (3M) (purple) and as-synthesized H_2SO_4@MIL-101-SO_3H (3M) washed by water for acid elimination (wine).

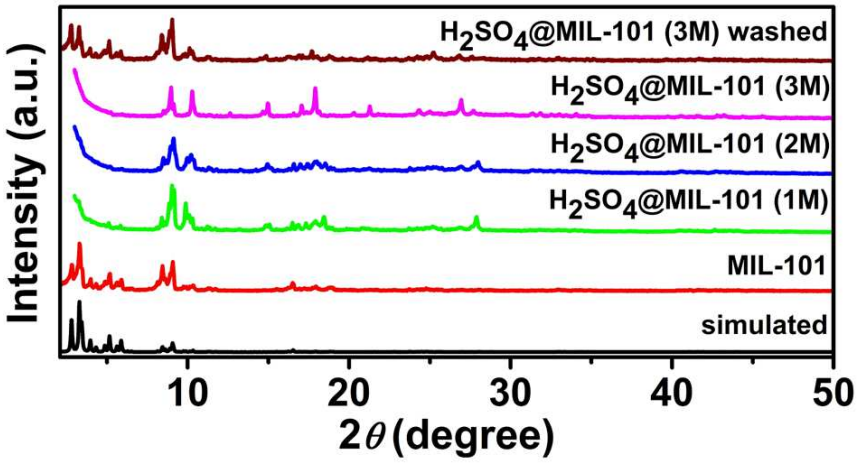

Figure S2 PXRD patterns of simulated MIL-101 (black), as-synthesized MIL-101 (red), as-synthesized H_2SO_4@MIL-101 (1M) (green), as-synthesized H_2SO_4@MIL-101 (2M) (blue), as-synthesized H_2SO_4@MIL-101 (3M) (purple) and as-synthesized H_2SO_4@MIL-101 (3M) washed by water for acid elimination (wine).

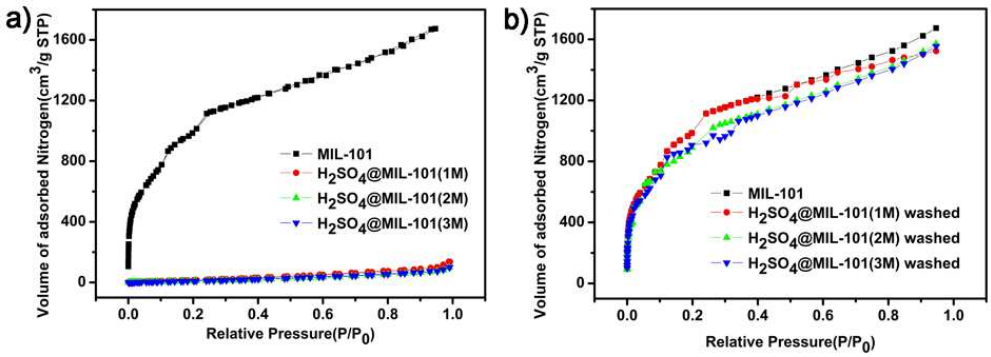

Figure S3 (a) N_2 adsorption-desorption isotherms of as-synthesized MIL-101 (black), as-synthesized H_2SO_4@MIL-101 (1M) (red), as-synthesized H_2SO_4@MIL-101 (2M) (green) and as-synthesized H_2SO_4@MIL-101 (3M) (blue) measured at 77K. (b) N_2 adsorption-desorption isotherms of as-synthesized MIL-101 (black), as-synthesized H_2SO_4@MIL-101 (1M) (red, washed), as-synthesized H_2SO_4@MIL-101 (2M) (green, washed) and H_2SO_4@MIL-101 (3M) (blue, washed) measured at 77K.

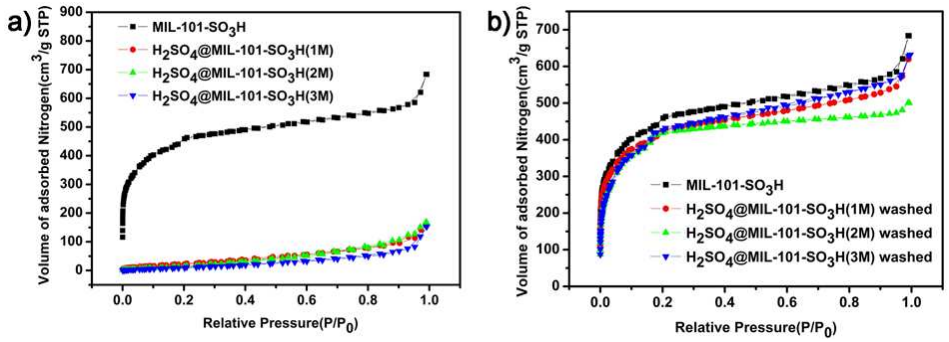

Figure S4 (a) N_2 adsorption-desorption isotherms of as-synthesized MIL-101-SO_3H (black), as-synthesized H_2SO_4@MIL-101-SO_3H (1M) (red), as-synthesized H_2SO_4@MIL-101-SO_3H (2M) (green) and H_2SO_4@MIL-101-SO_3H (3M) (blue) measured at 77K. (b) N_2 adsorption-desorption isotherms of as-synthesized MIL-101-SO_3H (black), as-synthesized H_2SO_4@MIL-101-SO_3H (1M) (red, washed), as-synthesized H_2SO_4@MIL-101-SO_3H (2M) (green, washed) and H_2SO_4@MIL-101-SO_3H (3M) (blue, washed) measured at 77K.

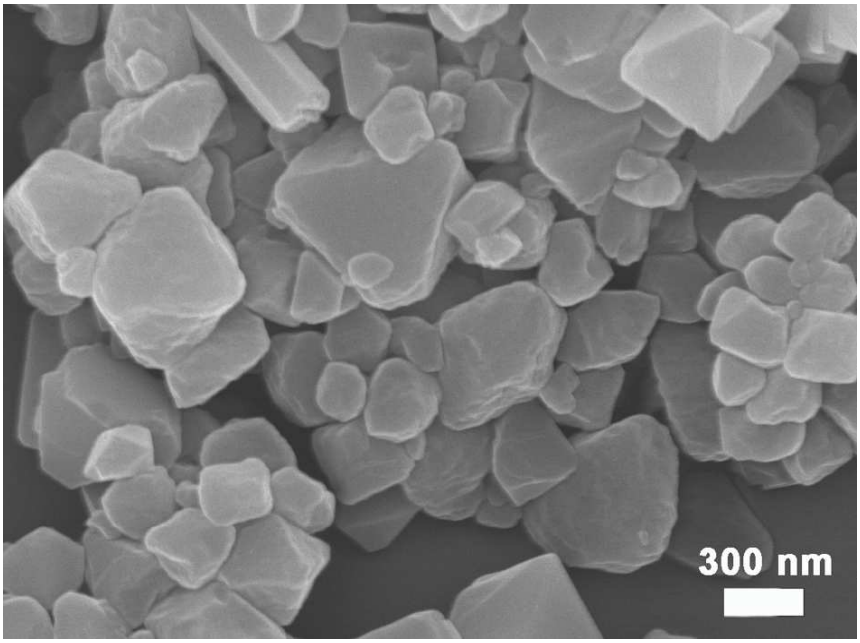

Figure S5 SEM imagine of as-synthesized MIL-101.

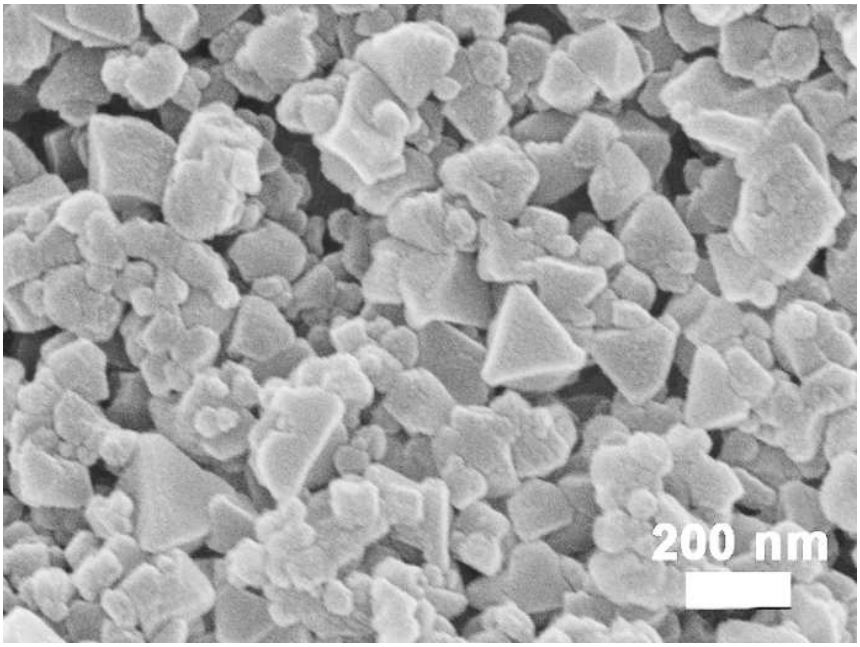

Figure S6 SEM imagine of as-synthesized MIL-101-SO_3H.

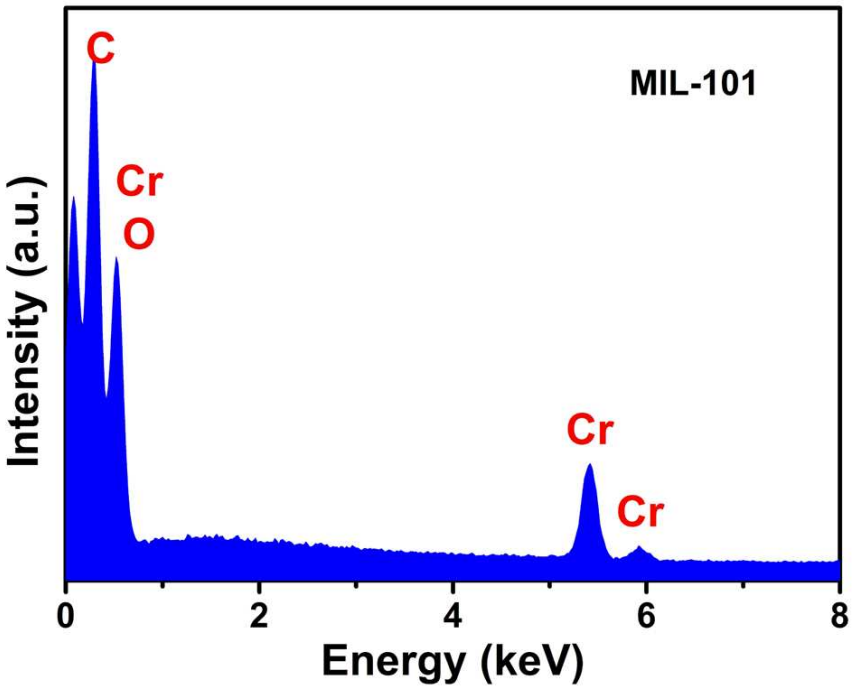

Figure S7 EDX spectrum of MIL-101.

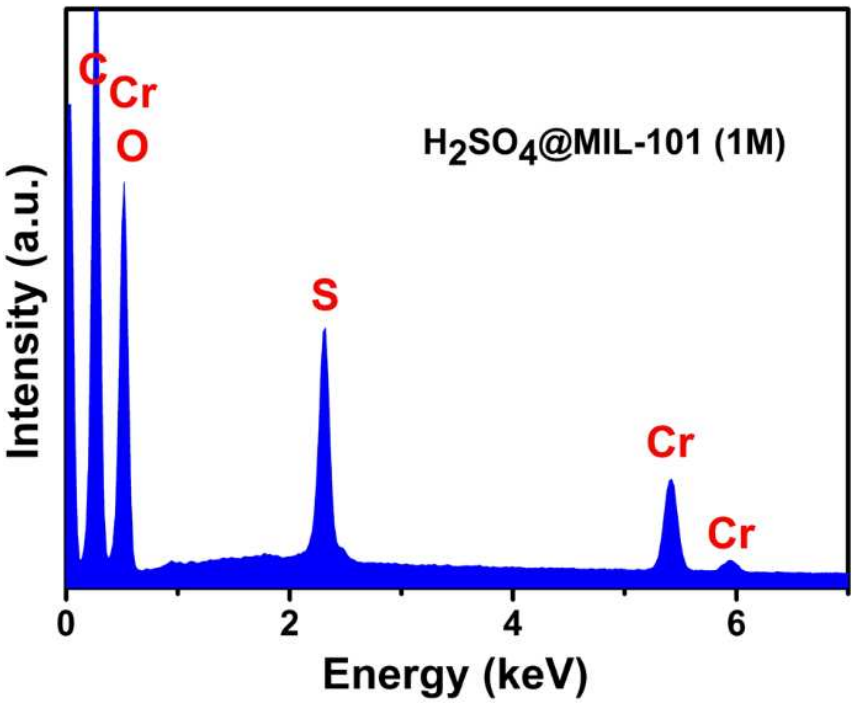

Figure S8 EDX spectrum of H_2SO_4@MIL-101 (1M).

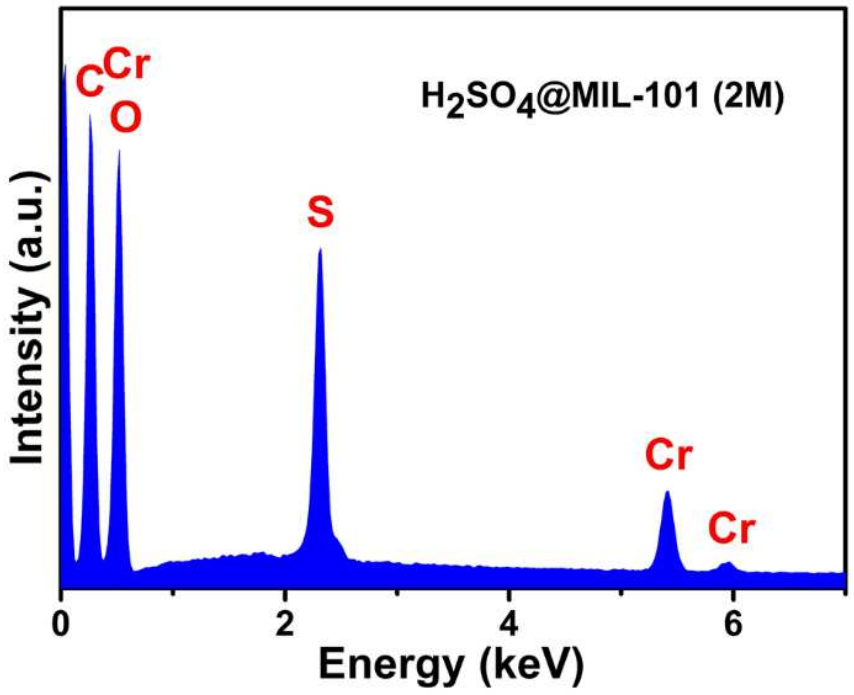

Figure S9 EDX spectrum of H_2SO_4@MIL-101 (2M).

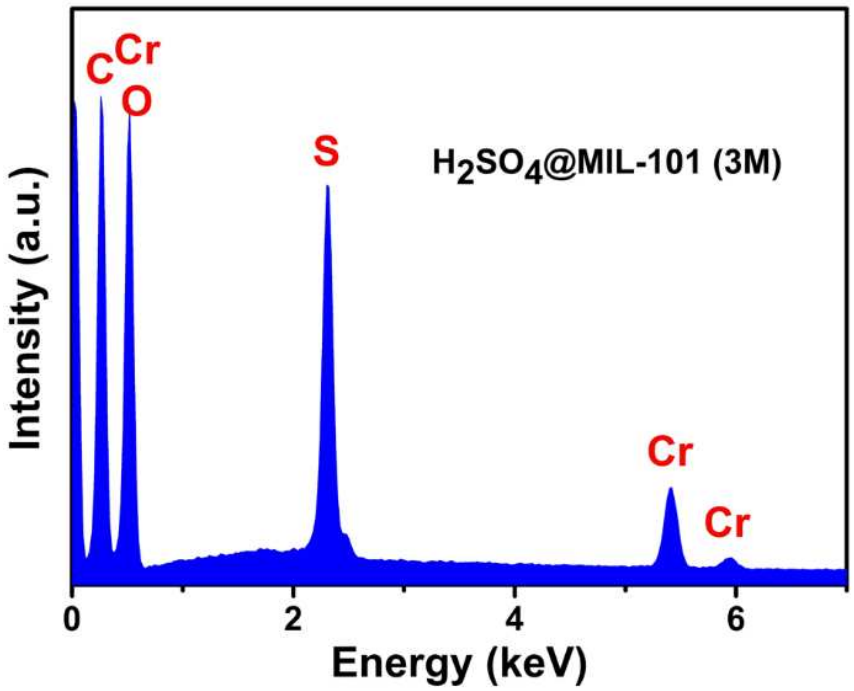

Figure S10 EDX spectrum of H_2SO_4@MIL-101 (3M).

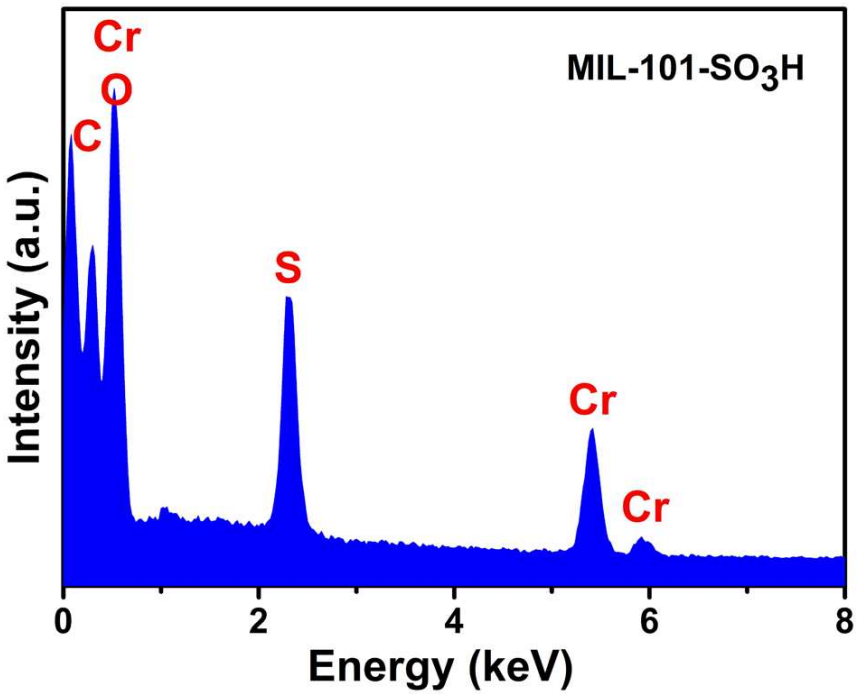

Figure S11 EDX spectrum of MIL-101-SO_3H.

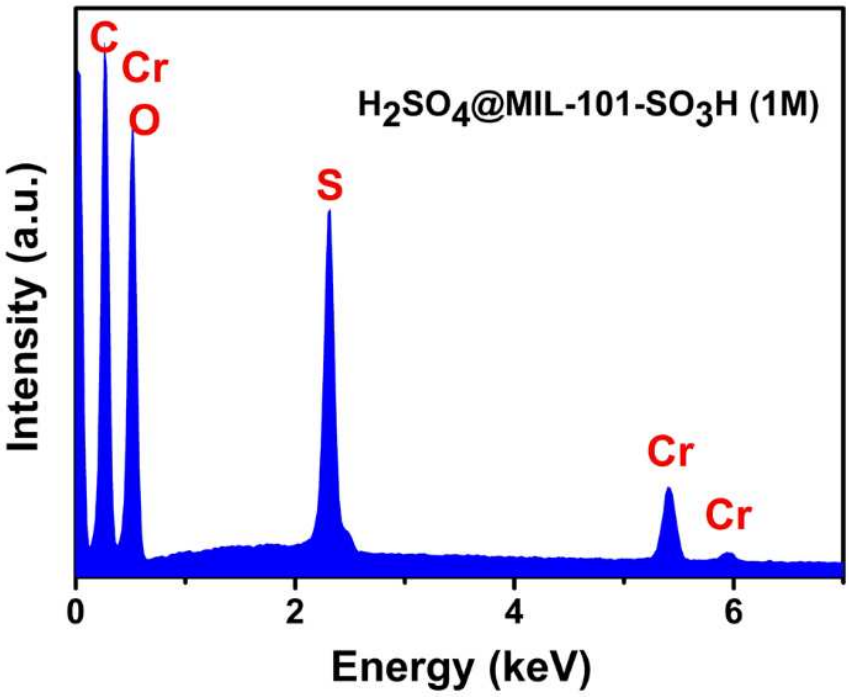

Figure S12 EDX spectrum of H_2SO_4@MIL-101-SO_3H (1M).

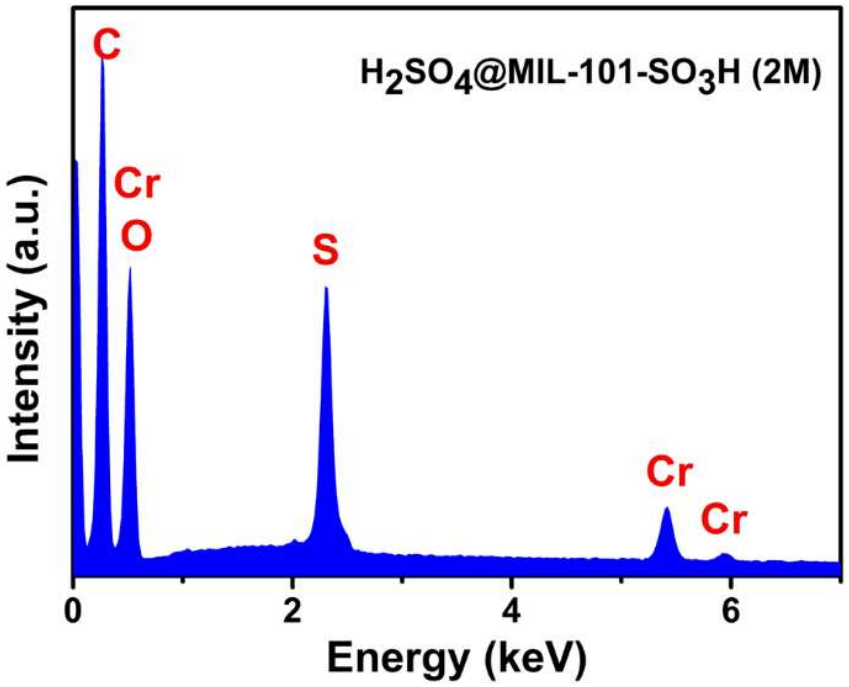

Figure S13 EDX spectrum of H_2SO_4@MIL-101-SO_3H (2M).

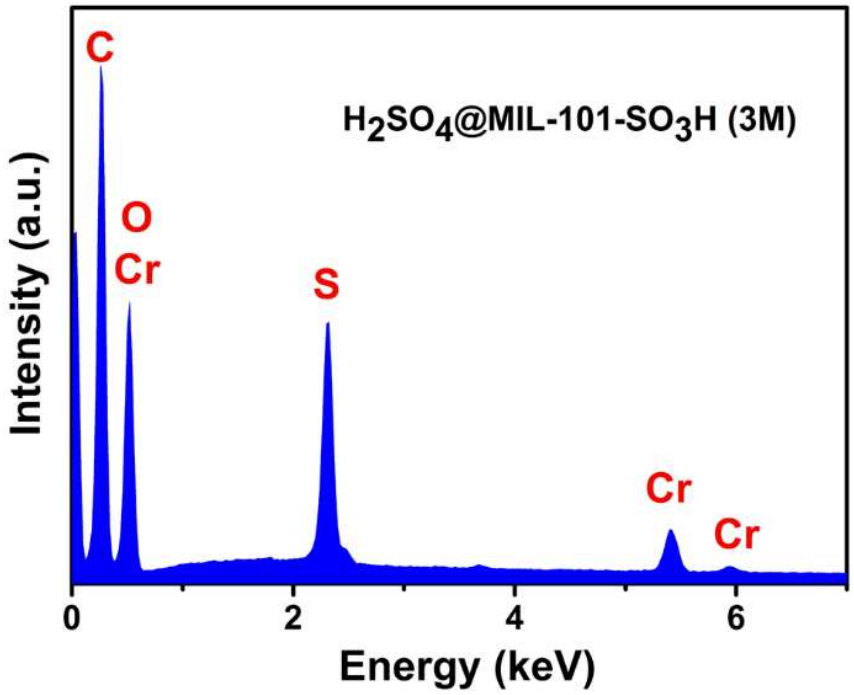

Figure S14 EDX spectrum of H_2SO_4@MIL-101-SO_3H (3M).

2. Proton conductivity characterization

The samples were put into a homemade mould with a diameter of 0.2 cm radius to get circular pellets. The thickness was measured by a vernier caliper. And then the pellets were smeared by silver colloid on two sides which were fixed on the sample stage with gold wires. The proton conductivities were measured on the pellets using a quasi-four-probe method with an impedance/gain-phase analyzer (Solartron S1 1260) over a frequency range from 1 Hz to 1 MHz with an input voltage of 300 mV (except an input voltage of 3000 mV was exclusively used for MIL-101-SO_3H because of a more smooth semicircle than with 300 mV). The measurements were operated at subzero temperatures (-10 to -40°C) and 30°C, different relative humidities (40% to 90%RH). Therein, longer retention time (2 hours) at per temperature of cycle measurement to get closer to the final equilibrium state was executed. The proton conductivity was calculated using the following equation

$$\sigma = \frac{l}{SR}$$

where σ is the conductivity (S cm^{-1}), l is the thickness (cm) of the pellet, S is the cross-sectional area (cm^2) of the pellet and R is the bulk resistance (Ω). The activation energy (E_a) was calculated from the following equation

$$\ln(\sigma T) = \ln \sigma_0 - \frac{E_a}{KT} \qquad (K=8.6\times10^{-5}\ \text{eV/K})$$

where σ is the conductivity (S cm^{-1}), K is the Boltzmann constant (eV/K) and T is the temperature (K). ZView software was used to measure bulk resistance through an equivalent circuit simulation to get the Nyquist plots and resistance values by fitting the semicircles.

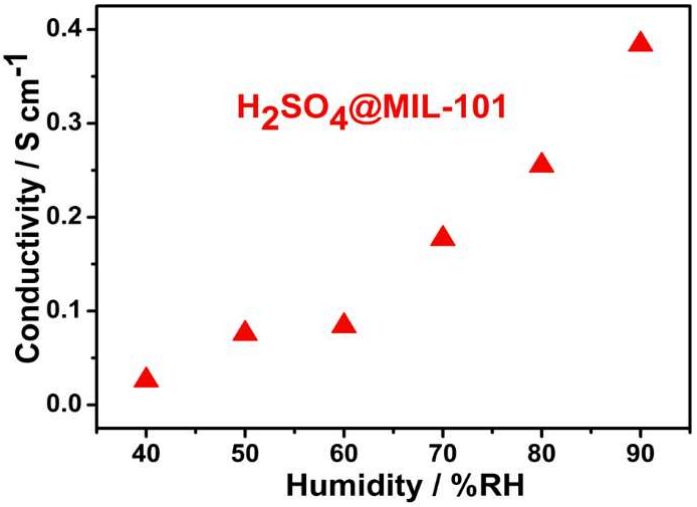

Figure S15 The values of proton conductivity of H_2SO_4@MIL-101 (3M) at 30°C and different humidities variation from 40% to 90% RH.

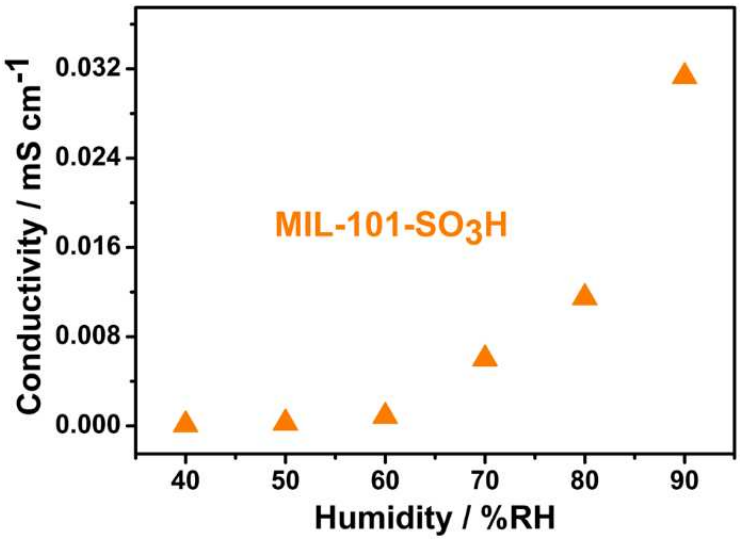

Figure S16 The values of proton conductivity of MIL-101-SO_3H at 30°C and different humidities variation from 40% to 90% RH.

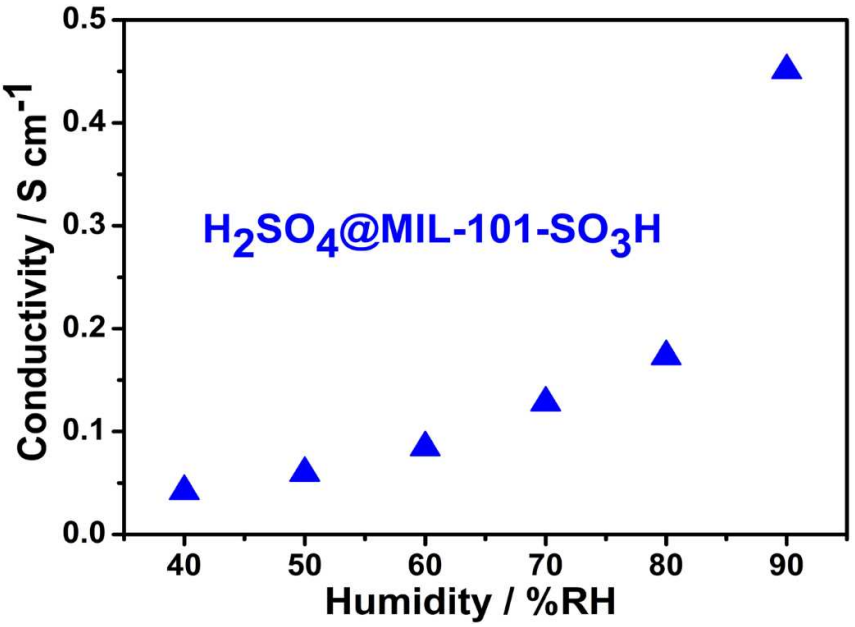

Figure S17 The values of proton conductivity of H_2SO_4@MIL-101-SO_3H (3M) at 30°C and different humidities variation from 40% to 90% RH.

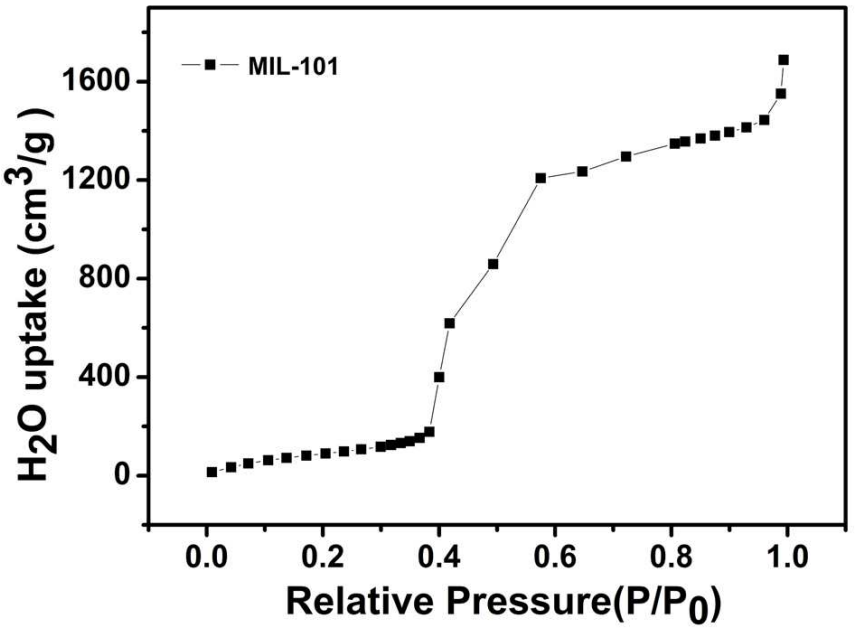

Figure S18 H_2O adsorption isotherms of as-synthesized MIL-101 measured at 298K.

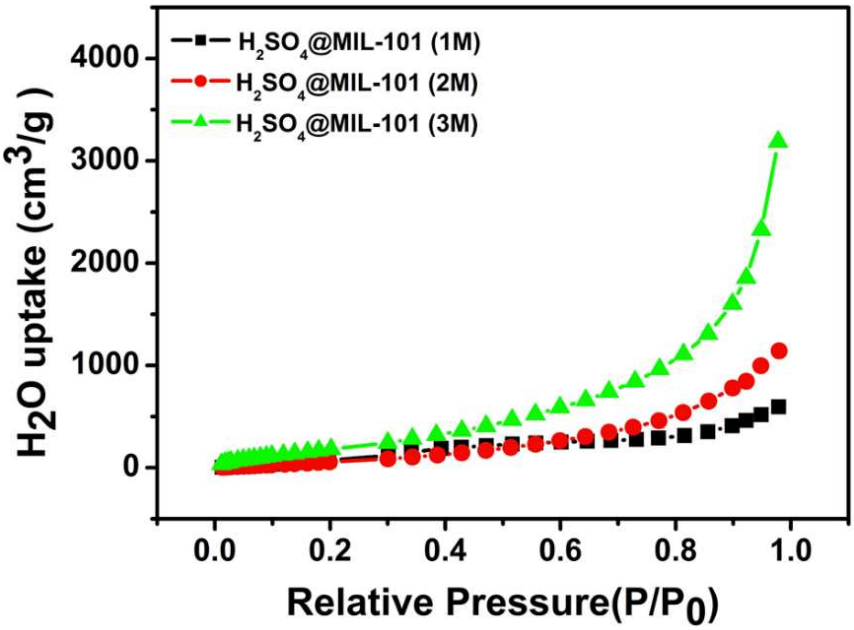

Figure S19 H_2O adsorption isotherms of as-synthesized H_2SO_4@MIL-101 (1M) (black), as-synthesized H_2SO_4@MIL-101 (2M) (red) and as-synthesized H_2SO_4@MIL-101 (3M) (green) measured at 298K.

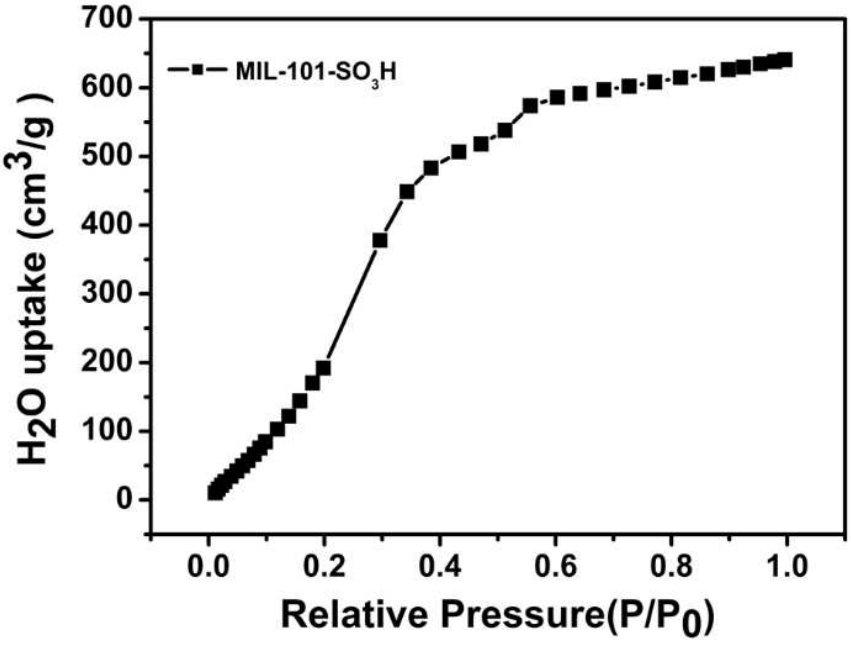

Figure S20 H_2O adsorption isotherm of as-synthesized MIL-101-SO_3H (black) measured at 298K.

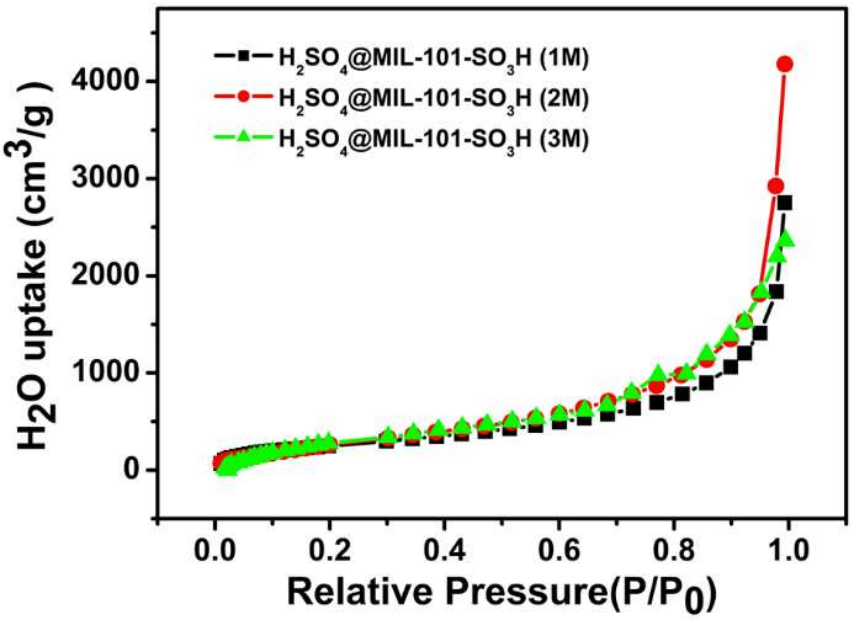

Figure S21 H_2O adsorption isotherms of as-synthesized H_2SO_4@MIL-101-SO_3H (1M) (black), as-synthesized H_2SO_4@MIL-101-SO_3H (2M) (red) and as-synthesized H_2SO_4@MIL-101-SO_3H (3M) (green) measured at 298K.

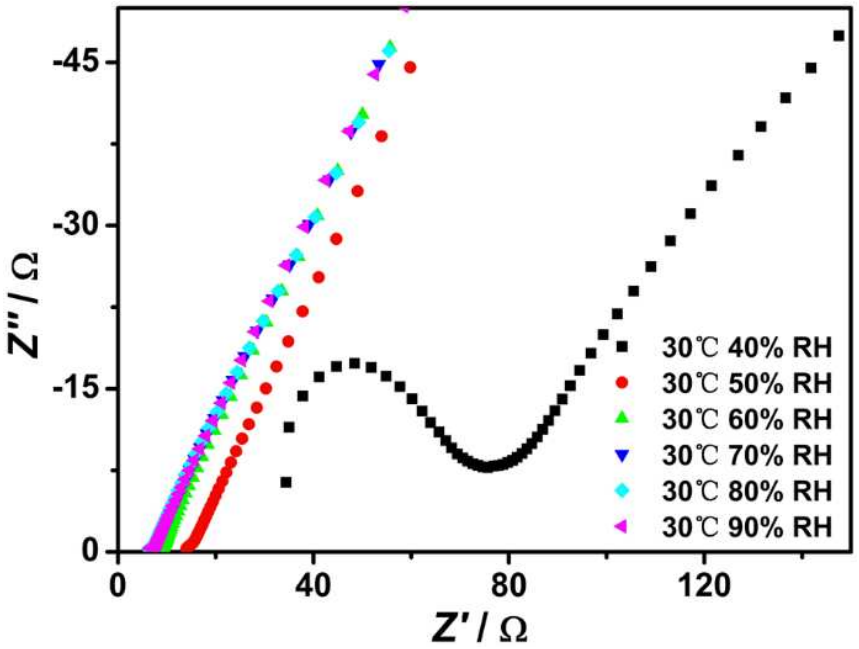

Figure S22 Nyquist plots from AC impedance data of H_2SO_4@MIL-101 (3M) at 30°C and different humidities variation from 40% to 90% RH.

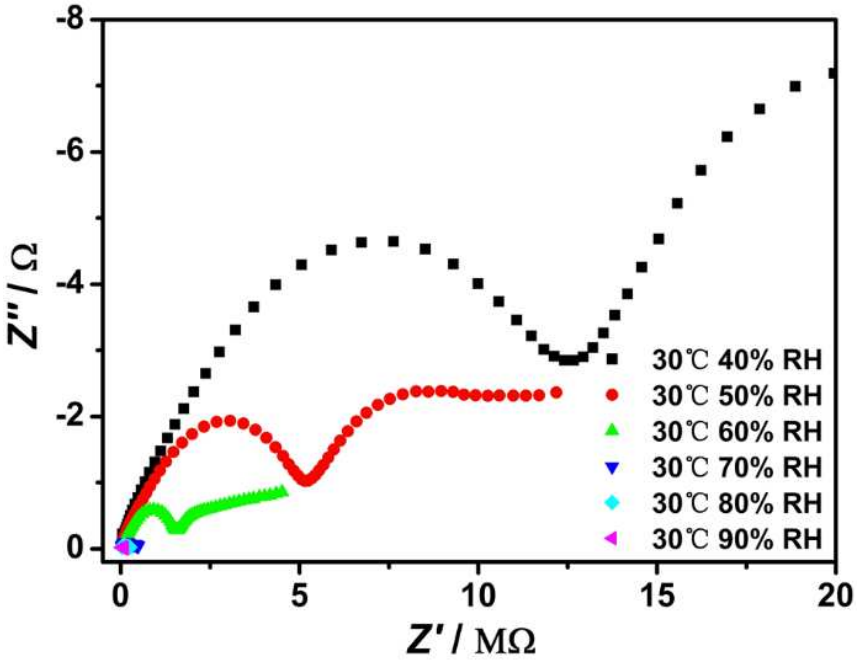

Figure S23 Nyquist plots from AC impedance data of MIL-101-SO_3H at 30°C and different humidities variation from 40% to 90% RH.

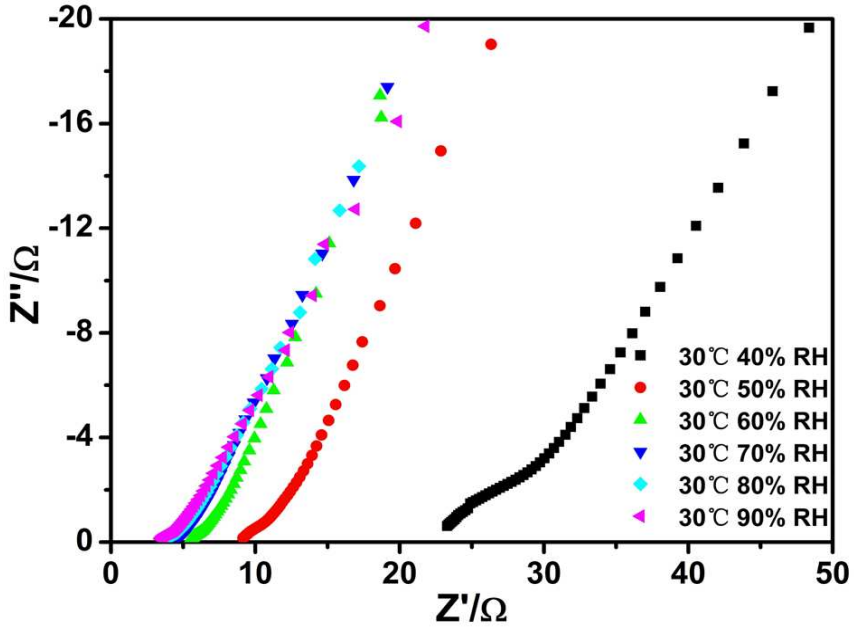

Figure S24 Nyquist plots from AC impedance data of H_2SO_4@MIL-101-SO_3H (3M) at 30°C and different humidities variation from 40% to 90% RH.

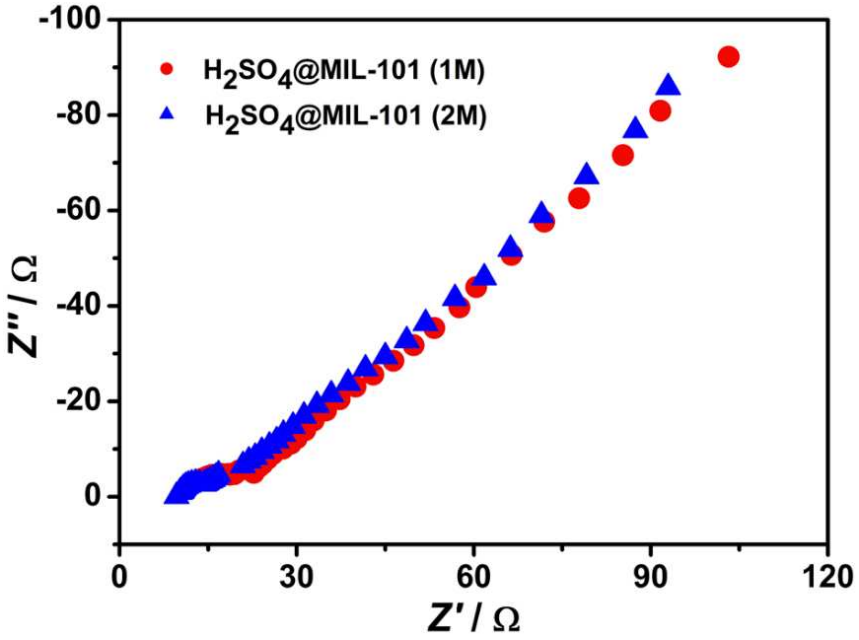

Figure S25 Nyquist plots from AC impedance data of H_2SO_4@MIL-101 (1M) (red) and H_2SO_4@MIL-101 (2M) (blue) at 30 °C and 90%RH.

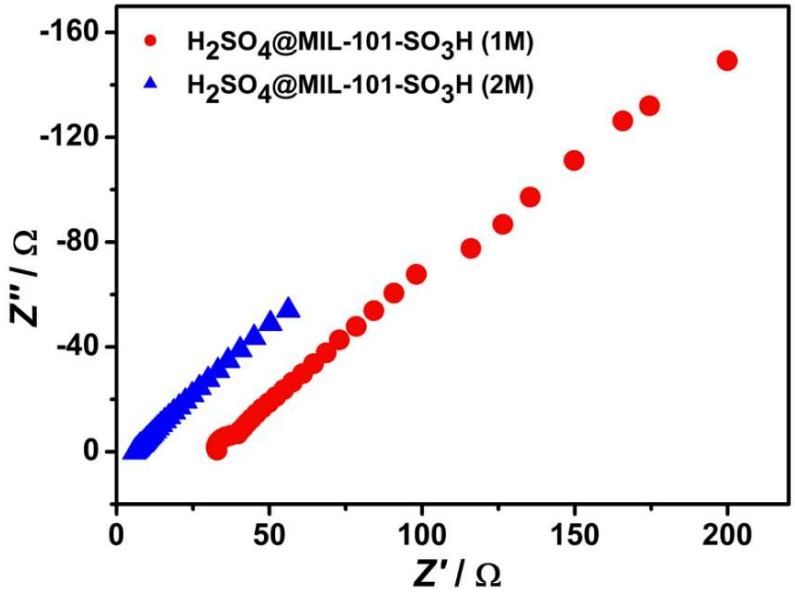

Figure S26 Nyquist plots from AC impedance data of H_2SO_4@MIL-101-SO_3H (1M) (red) and H_2SO_4@MIL-101 (2M) (blue) at 30 °C and 90%RH.

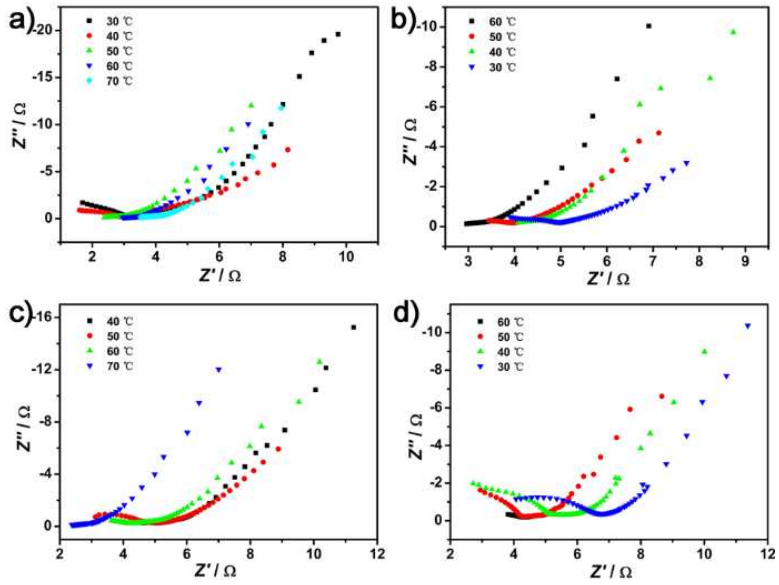

Figure S27 Nyquist plots from AC impedance data for the heating-cooling cycles of H_2SO_4@MIL-101 (3M) at 90%RH. (a) the first heating cycle (30-70 °C). (b) the first cooling cycle (60-30 °C). (c) the second heating cycle (40-70 °C). (d) the second cooling cycle (60-30 °C).

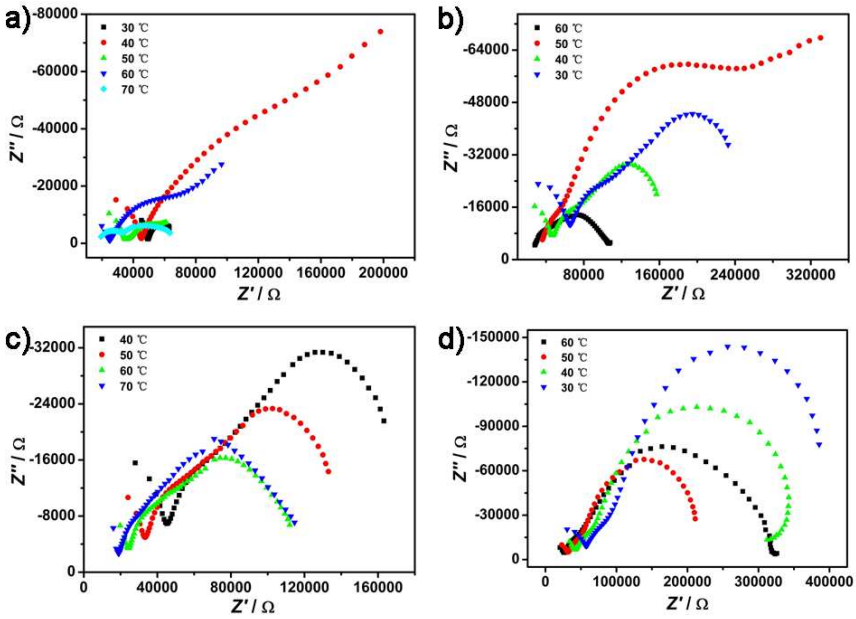

Figure S28 Nyquist plots from AC impedance data for the heating-cooling cycles of MIL-101-SO_3H at 90%RH. (a) the first heating cycle (30-70 °C). (b) the first cooling cycle (60-30 °C). (c) the second heating cycle (40-70 °C). (d) the second cooling cycle (60-30 °C).

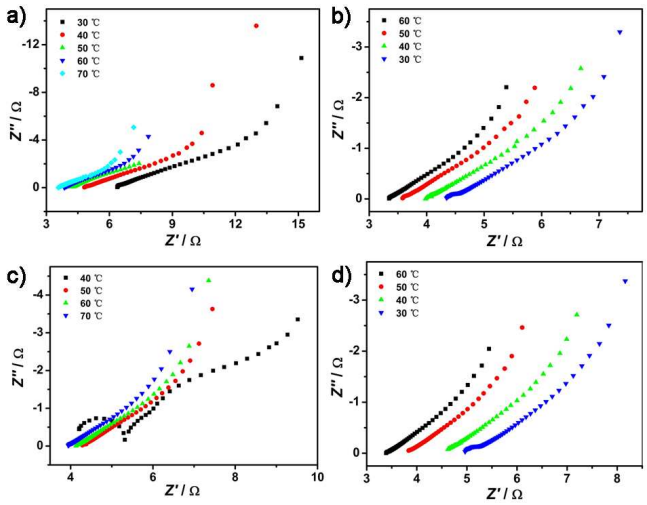

Figure S29 Nyquist plots from AC impedance data for the heating-cooling cycles of H_2SO_4@MIL-101-SO_3H (3M) at 90%RH. (a) the first heating cycle (30-70 °C). (b) the first cooling cycle (60-30 °C). (c) the second heating cycle (40-70 °C). (d) the second cooling cycle (60-30 °C).

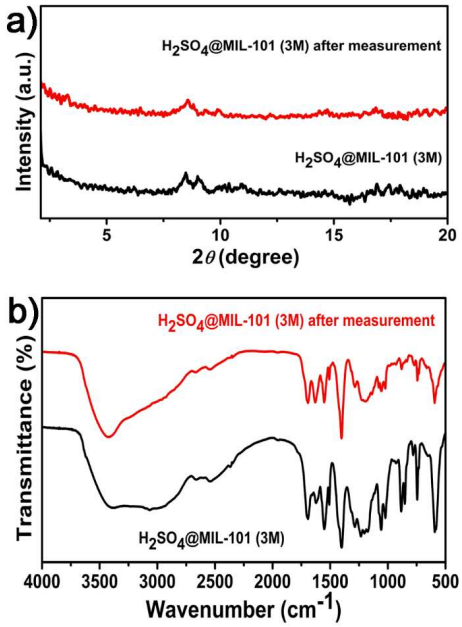

Figure S30 (a) PXRD patterns and (b) FT-IR spectra of as-synthesized H_2SO_4@MIL-101 (3M) (black) and H_2SO_4@MIL-101 (3M) undergoing two heating-cooling cycles conductivity measurements (red).

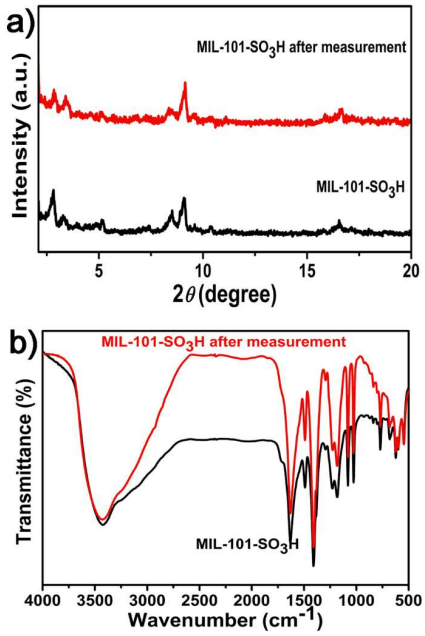

Figure S31 (a) PXRD patterns and (b) FT-IR spectra of as-synthesized MIL-101-SO_3H (black) and MIL-101-SO_3H undergoing two heating-cooling cycles conductivity measurements (red).

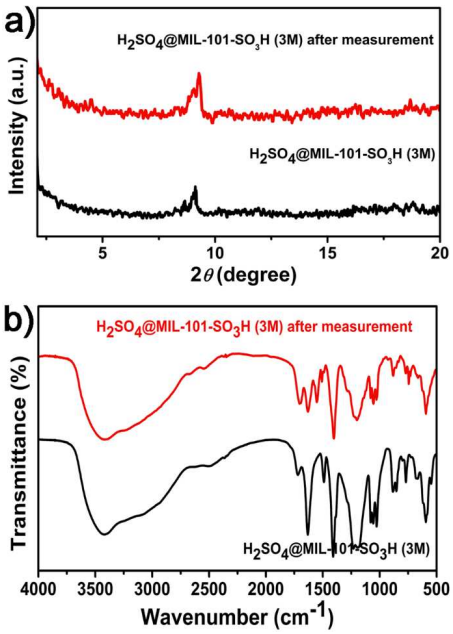

Figure S32 (a) PXRD patterns and (b) FT-IR spectra of as-synthesized H_2SO_4@MIL-101-SO_3H (3M) (black) and H_2SO_4@MIL-101-SO_3H (3M) undergoing two heating-cooling cycles conductivity measurements (red).

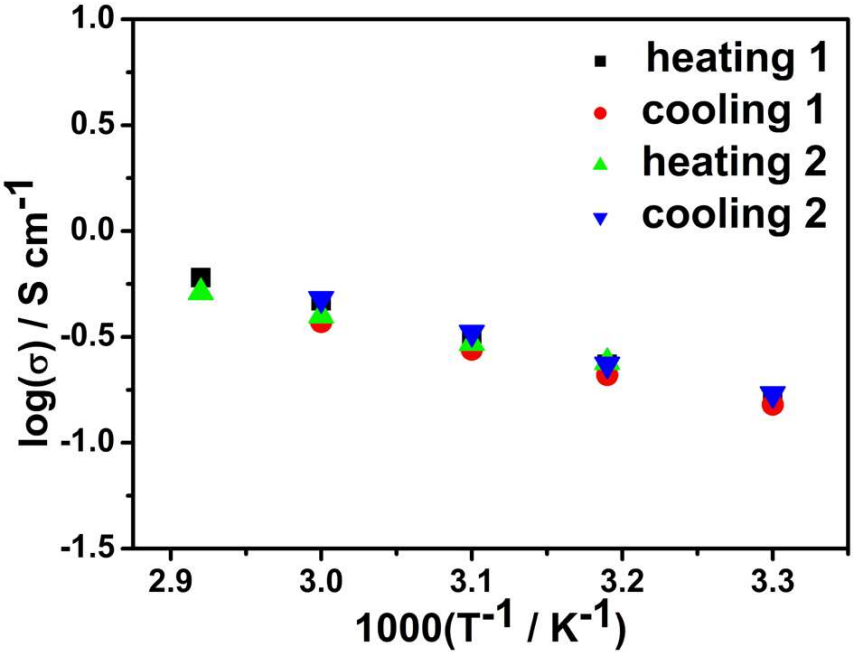

Figure S33 Log-scaled proton conductivities for the heating-cooling cycles of H_2SO_4@MIL-101 (3M) at 90%RH.

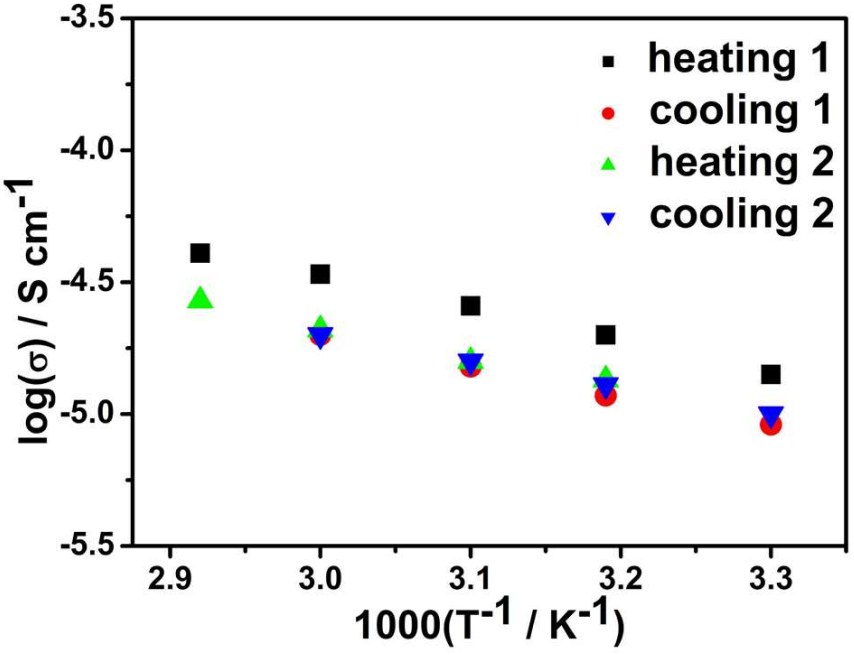

Figure S34 Log-scaled proton conductivities for the heating-cooling cycles of MIL-101-SO_3H at 90%RH.

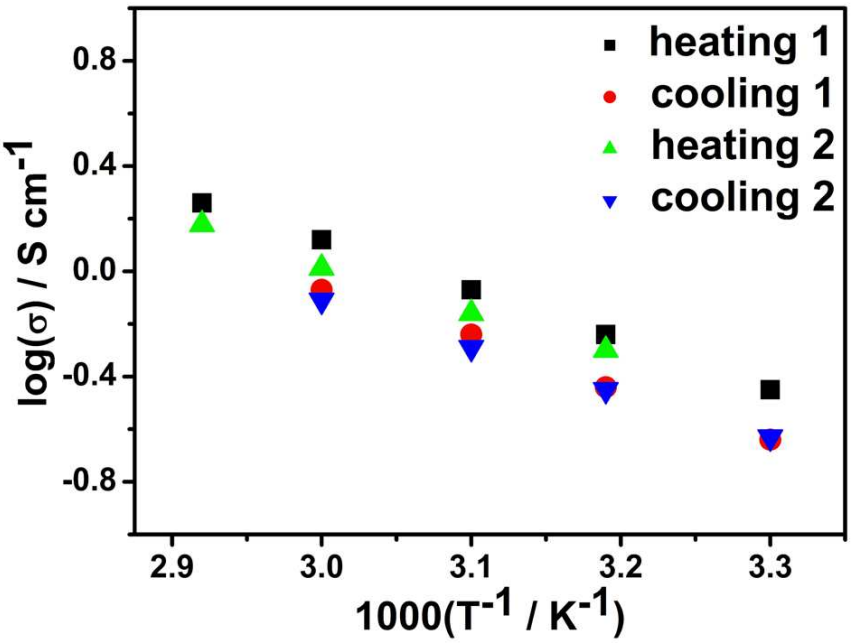

Figure S35 Log-scaled proton conductivities for the heating-cooling cycles of H_2SO_4@MIL-101-SO_3H (3M) at 90%RH.

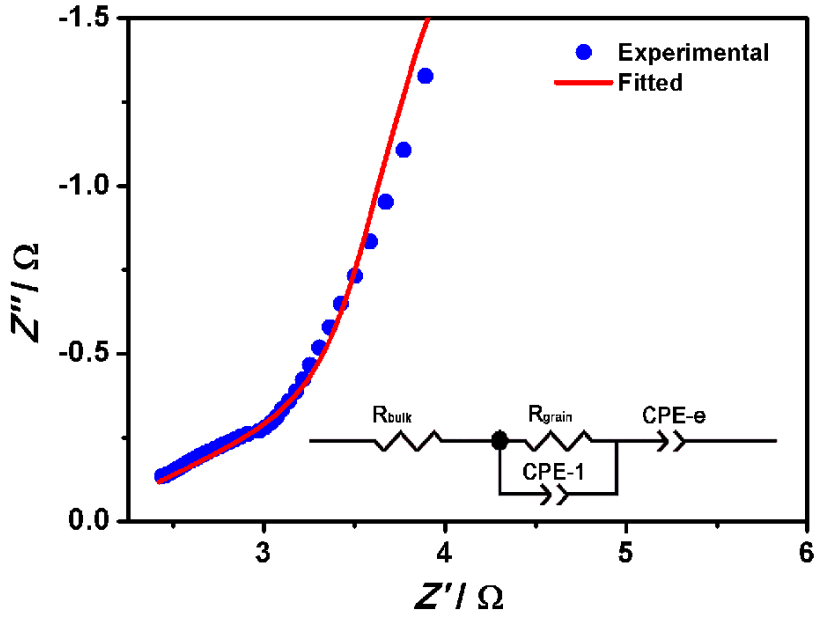

Figure S36 Fitting for the Nyquist plot at 70 °C and 90%RH, with circuit model used for the data fitting shown as an inset.

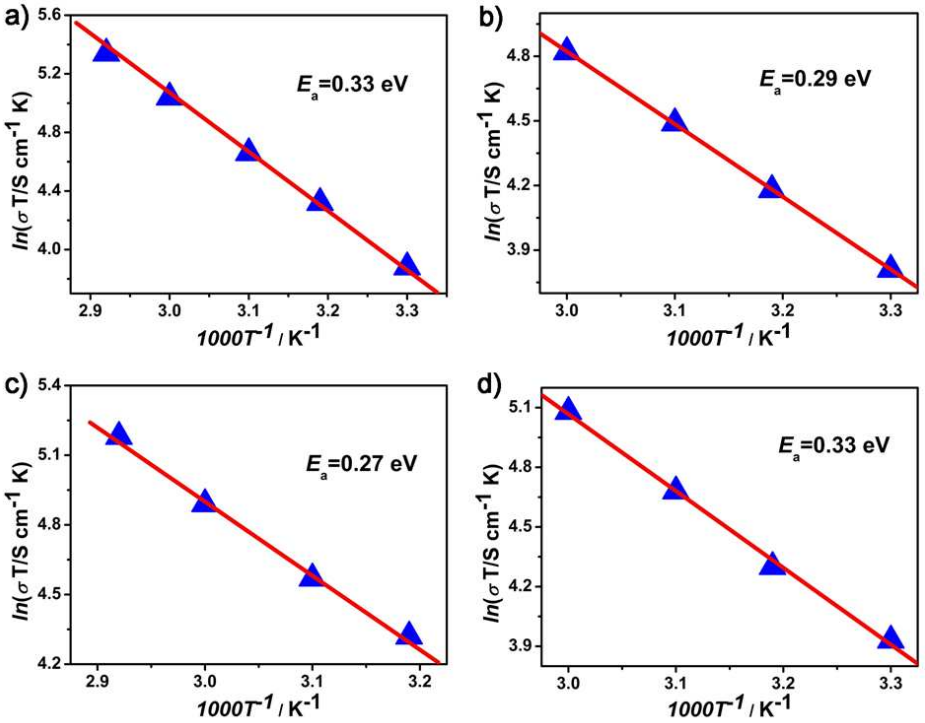

Heating 1 (°C)	R1	R2	R3 (S^{-1})	$R'_{average}$ (S^{-1})	Fitting Parameter (Y=A+B*X)		
30	5.6226	5.6391	5.8398	5.7005	Parameter	Value	Error
40	3.5996	3.6059	4.3136	3.8397	A	16.54037	0.08839
50	2.6914	2.7624	2.9204	2.7914	B	-3.83378	0.02847
60	1.8756	2.0058	2.0148	1.9654	R_{fit}=-0.99992		
70	1.4702	1.4921	1.5170	1.4931			
Cooling 1 (°C)							
60	2.4187	2.4267	2.5079	2.4511	Parameter	Value	Error
50	3.1897	3.3216	3.4160	3.3091	A	14.9428	0.05713
40	4.3056	4.3817	4.4377	4.3750	B	-3.37341	0.01814
30	6.0432	6.0712	6.0782	6.0642	R_{fit}=-0.99997		
Heating 2 (°C)							
40	3.7954	3.8162	3.8209	3.8075	Parameter	Value	Error
50	3.0433	3.0512	3.0666	3.0537	A	14.45501	0.3811
60	2.1549	2.2996	2.3876	2.2807	B	-3.18264	0.12478
70	1.7526	1.7533	1.7747	1.7602	R_{fit}=-0.99847		

Cooling 2 (°C)							
60	1.8724	1.8906	1.9010	1.8880	Parameter	Value	Error
50	2.6102	2.6755	2.9124	2.7327	A	16.65298	0.4193
40	3.7640	3.9020	3.9509	3.8723	B	-3.86195	0.13313
30	5.3701	5.3825	5.4012	5.3846	R_{fit}=-0.99881		

Figure S37 Arrhenius plots of H_2SO_4@MIL-101 (3M) for the every heating-cooling cycle (at the temperature range of 30-70 °C and 90%RH). (a) the first heating cycle (30-70 °C). (b) the first cooling cycle (60-30 °C). (c) the second heating cycle (40-70 °C). (d) the second cooling cycle (60-30 °C). The fitting line (red line) is shown to calculate the value of E_a.

Below: The table shows corresponding fitting parameters including R (the resistances from Nyquist plots, respectively), $R'_{average}$ (average resistance), A (intercept of fitting line), B (slope of fitting line) and R_{fit} (The closer the R value is to 1, the better the degree of fitting is).

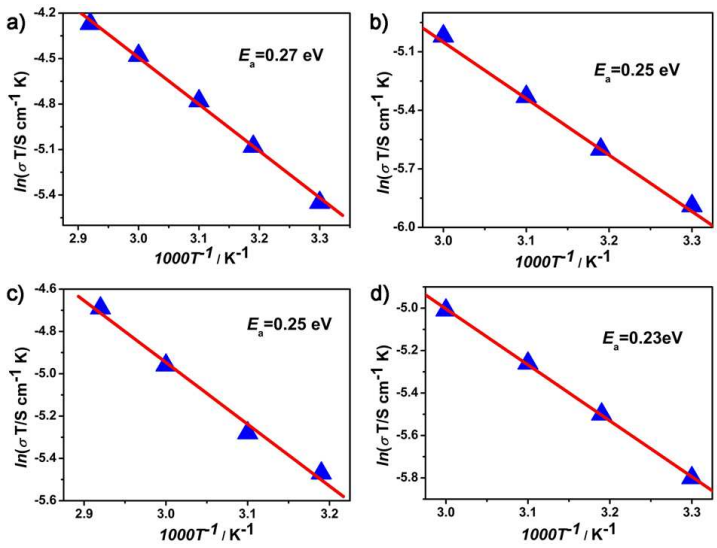

Heating 1 (°C)	R1	R2	R3 (S^{-1})	$R'_{average}$ (S^{-1})	Fitting Parameter (Y=A+B*X)		
30	58607	58742	60113	59154	Parameter	Value	Error
40	40135	43218	43919	42424	A	4.87249	0.26471
50	30122	33256	33918	32432	B	-3.12202	0.08526
60	24002	25003	25113	24706	R_{fit}=-0.99888		
70	20105	20508	21304	20639			

Cooling 1 (°C)							
60	41584	42477	43211	42424	Parameter	Value	Error
50	50108	58231	59661	56000	A	3.68587	0.25415
40	70109	70234	73215	71186	B	-2.90576	0.0807
30	89704	92046	93059	91603	R_{fit}=-0.99923		
Heating 2 (°C)							
40	60114	63215	64732	62687	Parameter	Value	Error
50	50123	54657	55729	53503	A	3.81278	0.61911
60	37631	39156	43213	40000	B	-2.91983	0.20271
70	30015	32012	32356	31461	R_{fit}=-0.99521		
Cooling 2 (°C)							
60	38654	39657	47689	42000	Parameter	Value	Error
50	51021	52633	53846	52500	A	2.90837	0.12053
40	62120	65179	66546	64615	B	-2.63729	0.03827
30	80976	85431	85593	84000	R_{fit}=-0.99979		

Figure S38 Arrhenius plots of MIL-101-SO_3H for the every heating-cooling cycle (at the temperature range of 30-70 °C and 90%RH). (a) the first heating cycle (30-70 °C). (b) the first cooling cycle (60-30 °C). (c) the second heating cycle (40-70 °C). (d) the second cooling cycle (60-30 °C). The fitting line (red line) is shown to calculate the value of E_a.

Below: The table shows corresponding fitting parameters including R (the resistances from Nyquist plots, respectively), $R'_{average}$ (average resistance), A (intercept of fitting line), B (slope of fitting line) and R_{fit} (The closer the R value is to 1, the better the degree of fitting is).

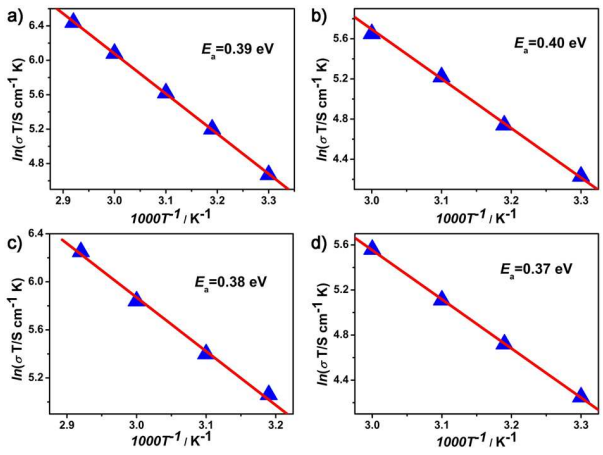

Heating 1 (°C)	R1	R2	R3 (S^{-1})	$R'_{average}$ (S^{-1})	Fitting Parameter (Y=A+B*X)		
30	1.7223	1.7518	1.7705	1.7482	Parameter	Value	Error
40	1.0698	1.0721	1.0816	1.0745	A	20.04303	0.1091
50	0.7211	0.7286	0.7412	0.7303	B	-4.65539	0.03514
60	0.4612	0.4586	0.5001	0.4733	R_{fit}=-0.99991		
70	0.3221	0.3471	0.3508	0.3400			
Cooling 1 (°C)							
60	0.7112	0.7376	0.7421	0.7303	Parameter	Value	Error
50	1.0687	1.0911	1.0976	1.0858	A	20.01926	0.40164
40	1.6478	1.7261	1.7360	1.7033	B	-4.78451	0.12753
30	2.7111	2.7316	2.7512	2.7313	R_{fit}=-0.99929		
Heating 2 (°C)							
40	1.2121	1.2402	1.2527	1.2350	Parameter	Value	Error
50	0.8400	0.8532	1.0368	0.9100	A	19.0674	0.60464
60	0.5921	0.6002	0.6134	0.6019	B	-4.39964	0.19797
70	0.3912	0.4195	0.4235	0.4114	R_{fit}=-0.99798		
Cooling 2 (°C)							
60	0.7600	0.8100	0.8300	0.7000	Parameter	Value	Error
50	1.2006	1.2117	1.2204	1.2109	A	18.64163	0.12053
40	1.7218	1.7358	1.7525	1.7367	B	-4.36271	0.03827
30	2.5916	2.6581	2.7304	2.6600	R_{fit}=-0.99992		

Figure S39 Arrhenius plots of H_2SO_4@MIL-101-SO_3H (3M) for the every heating-cooling cycle (at the temperature range of 30-70 ℃ and 90%RH). (a) the first heating cycle (30-70 °C). (b) the first cooling cycle (60-30 °C). (c) the second heating cycle (40-70 °C). (d) the second cooling cycle (60-30 °C). The fitting line (red line) is shown to calculate the value of E_a.

Below: The table shows corresponding fitting parameters including R (the resistances from Nyquist plots, respectively), $R'_{average}$ (average resistance), A (intercept of fitting line), B (slope of fitting line) and R_{fit} (The closer the R value is to 1, the better the degree of fitting is).

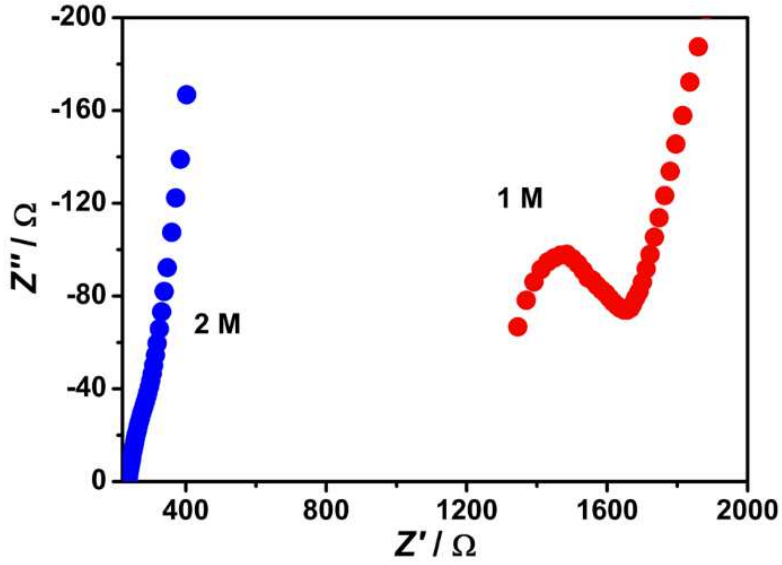

Figure S40 Nyquist plots from AC impedance data of H_2SO_4@MIL-101-SO_3H (1M) (red) and H_2SO_4@MIL-101-SO_3H (2M) (blue) at -40 °C.

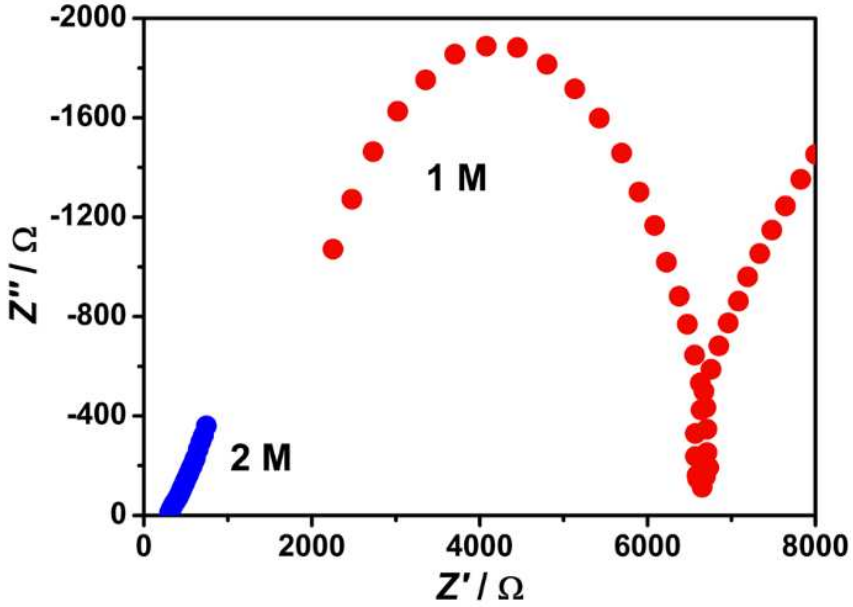

Figure S41 Nyquist plots from AC impedance data of H_2SO_4@MIL-101 (1M) (red) and H_2SO_4@MIL-101 (2M) (blue) at -40 °C.

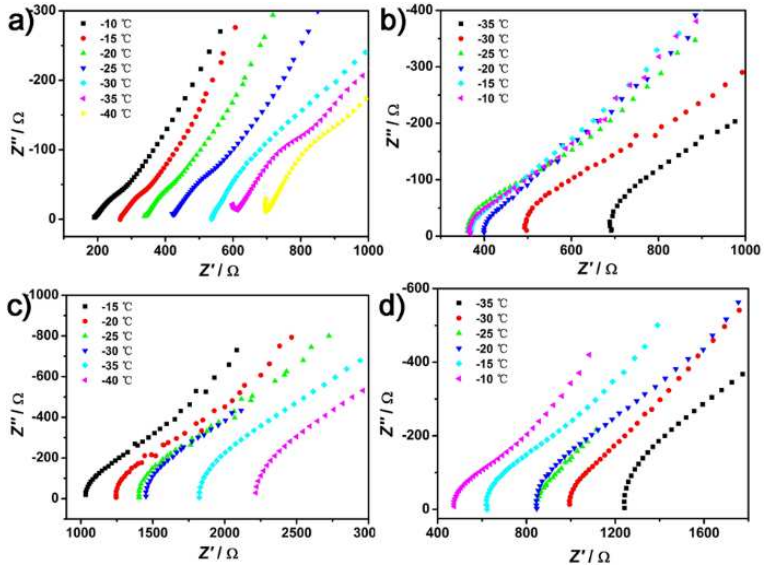

Figure S42 Nyquist plots from AC impedance data for the cooling-heating cycles of H_2SO_4@MIL-101 (3M) at subzero temperatures. (a) the first cooling cycle (-10--40 °C). (b) the first heating cycle (-35--10 °C). (c) the second cooling cycle (-15--40 °C). (d) the second heating cycle (-35--10 °C).

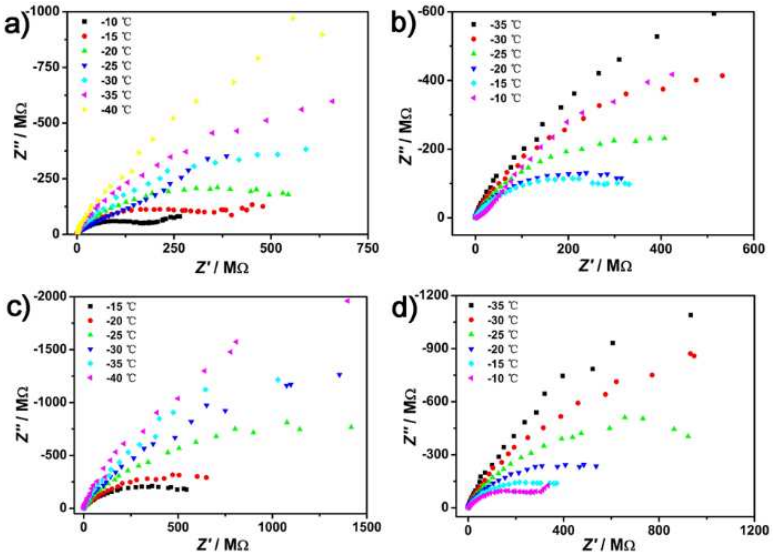

Figure S43 Nyquist plots from AC impedance data for the cooling-heating cycles of MIL-101-SO_3H at subzero temperatures. (a) the first cooling cycle (-10--40 °C). (b) the first heating cycle (-35--10 °C). (c) the second cooling cycle (-15--40 °C). (d) the second heating cycle (-35--10 °C).

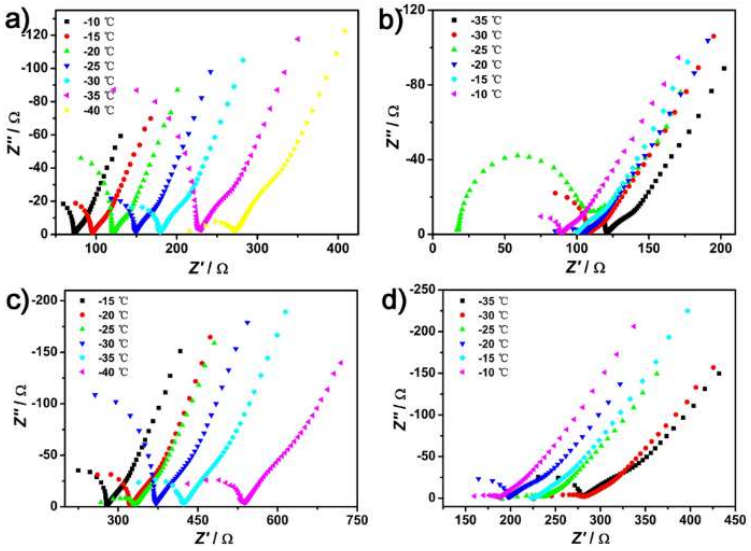

Figure S44 Nyquist plots from AC impedance data for the cooling-heating cycles of H_2SO_4@MIL-101-SO_3H (3M) at subzero temperatures. (a) the first cooling cycle (-10--40 °C). (b) the first heating cycle (-35--10 °C). (c) the second cooling cycle (-15--40 °C). (d) the second heating cycle (-35--10 °C).

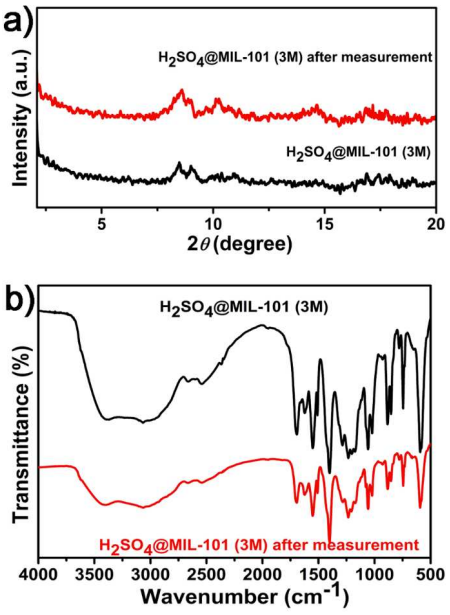

Figure S45 (a) PXRD patterns and (b) FT-IR spectra of as-synthesized H_2SO_4@MIL-101 (3M) (black) and H_2SO_4@MIL-101 (3M) undergoing two cooling-heating cycles conductivity measurements (red).

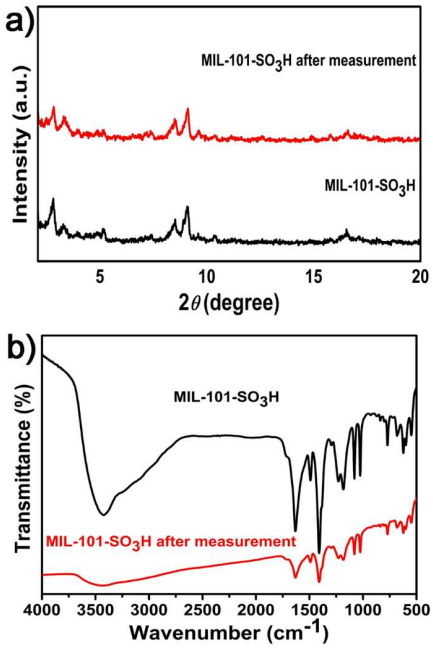

Figure S46 (a) PXRD patterns and (b) FT-IR spectra of as-synthesized MIL-101-SO_3H (black) and MIL-101-SO_3H undergoing two cooling-heating cycles conductivity measurements (red).

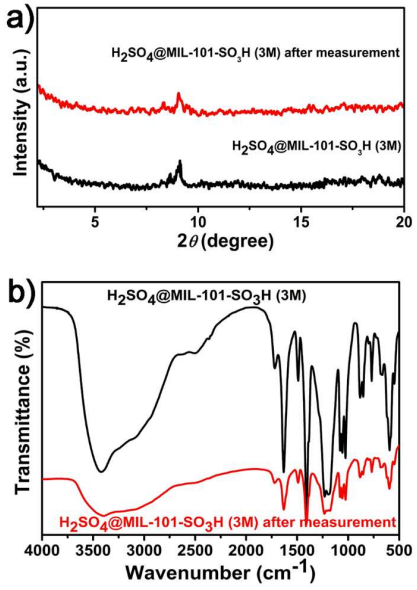

Figure S47 (a) PXRD patterns and (b) FT-IR spectra of as-synthesized H_2SO_4@MIL-101-SO_3H (3M) (black) and H_2SO_4@MIL-101-SO_3H (3M) undergoing two cooling-heating cycles conductivity measurements (red).

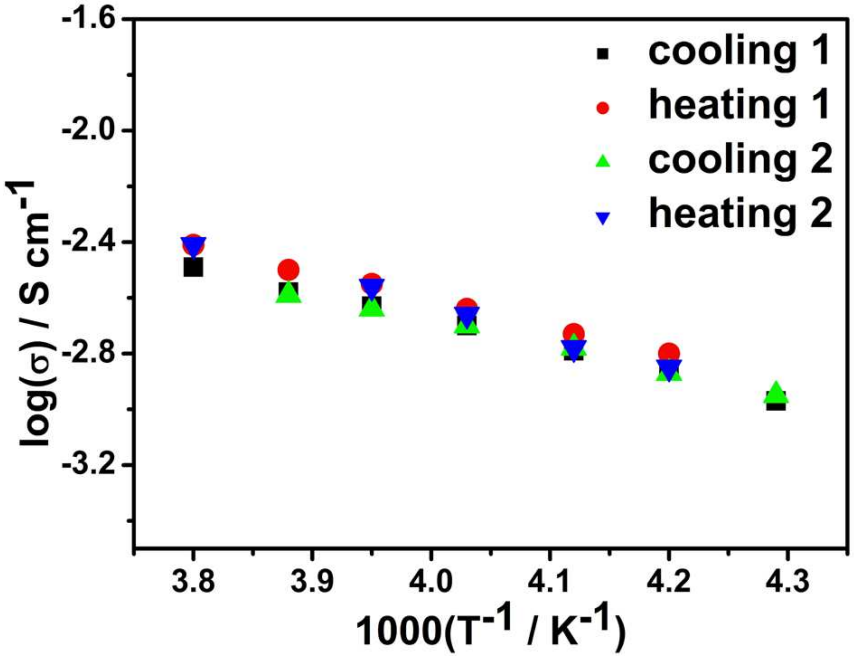

Figure S48 Log-scaled proton conductivities for the cooling-heating cycles of H_2SO_4@MIL-101 (3M) at subzero temperatures.

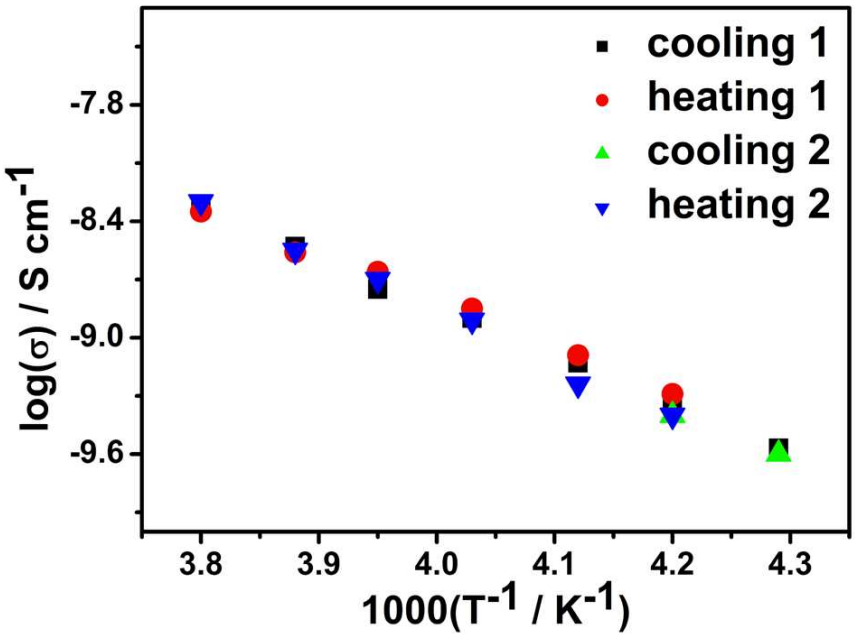

Figure S49 log-scaled proton conductivities for the cooling-heating cycles of MIL-101-SO_3H at subzero temperatures.

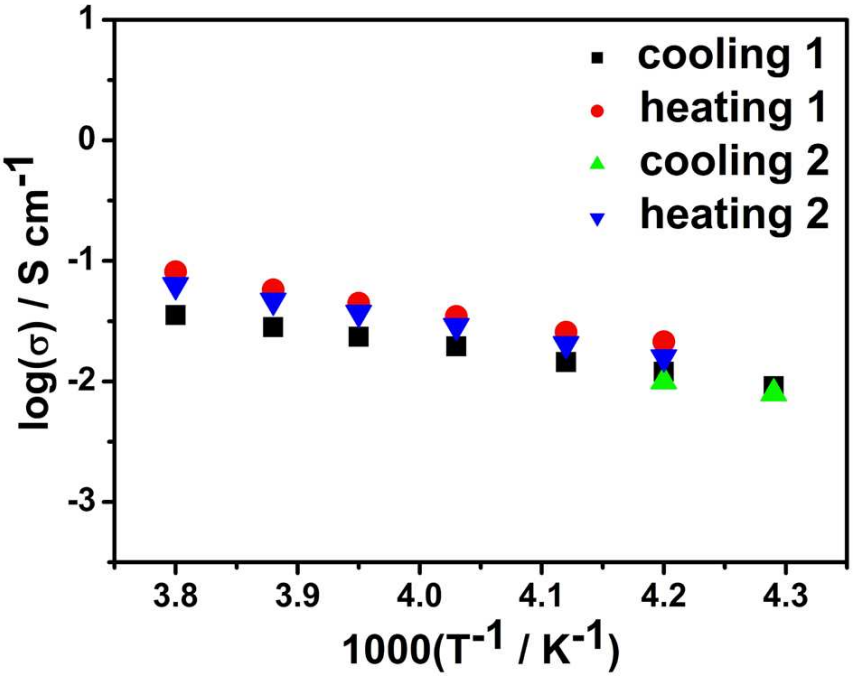

Figure S50 Log-scaled proton conductivities for the cooling-heating cycles of H_2SO_4@MIL-101-SO_3H (3M) at subzero temperatures.

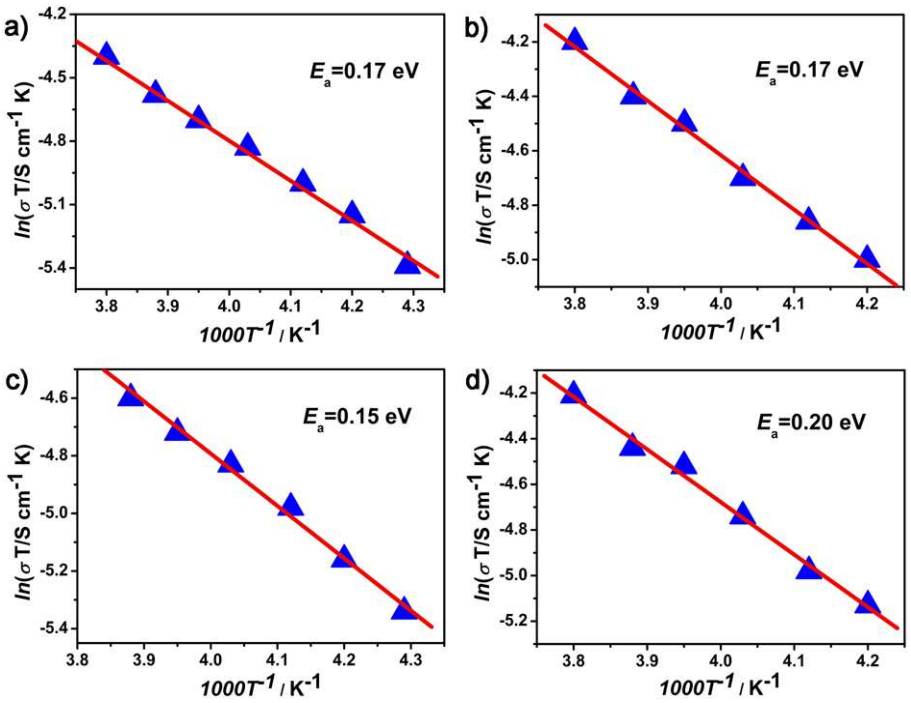

Cooling 1 (°C)	R1	R2	R3 (S^{-1})	$R'_{average}$ (S^{-1})	Fitting Parameter (Y=A+B*X)		
-10	275.67	290.14	330.41	298.74	Parameter	Value	Error
-15	347.35	356.305	391.405	365.02	A	2.95804	0.25165
-20	379.74	413.495	447.25	413.495	B	-1.9369	0.06226
-25	465.58	468.34	513.31	482.41			
-30	520.99	560.56	585.33	588.96	R_{fit}=-0.99743		
-35	690.42	695.865	701.31	695.865			
-40	812.34	849.74	1054.9	905.66			
Heating 1 (°C)							
-35	566.38	589.81	643.81	600	Parameter	Value	Error
-30	482.15	518.04	547.41	512.53	A	3.35244	0.26209
-25	394.75	410.34	463.64	422.91	B	0.06554	-1.99227
-20	325.87	333.63	361.79	340.43			
-15	298.71	305.15	310.42	304.76	R_{fit}=-0.99784		
-10	222.03	248.64	262.14	244.27			
Cooling 2 (°C)							
-15	346.31	383.82	386.14	372.09	Parameter	Value	Error
-20	399.8	409.17	459.76	422.91	A	2.36899	0.29521
-25	454.93	491.68	500.62	482.41	B	-1.79174	0.07234
-30	564.71	569.45	599.77	578.31			
-35	672.66	676.32	768.66	705.88	R_{fit}=-0.99676		
-40	803.53	850.8	940.25	864.86			
Heating 2 (°C)							
-35	658.33	664.11	738.1	686.85	Parameter	Value	Error
-30	556.77	561.44	620.48	579.56	A	4.53992	0.38434
-25	425.7	445.57	452.57	441.28	B	-2.3044	0.09611
-20	346.99	347.32	347.77	347.36			
-15	296.83	329.21	323.4	316.48	R_{fit}=-0.99654		
-10	223.29	256.47	264.7	248.15			

Figure S51 Arrhenius plots of H_2SO_4@MIL-101 (3M) for the every cooling-heating cycle (at subzero temperatures). (a) the first cooling cycle (-10--40 °C). (b) the first heating cycle (-35--

10 °C). (c) the second cooling cycle (-15--40 °C). (d) the second heating cycle (-35--10 °C). The fitting line (red line) is shown to calculate the value of E_a.

Below: The table shows corresponding fitting parameters including R (the resistances from Nyquist plots, respectively), $R'_{average}$ (average resistance), A (intercept of fitting line), B (slope of fitting line) and R_{fit} (The closer the R value is to 1, the better the degree of fitting is).

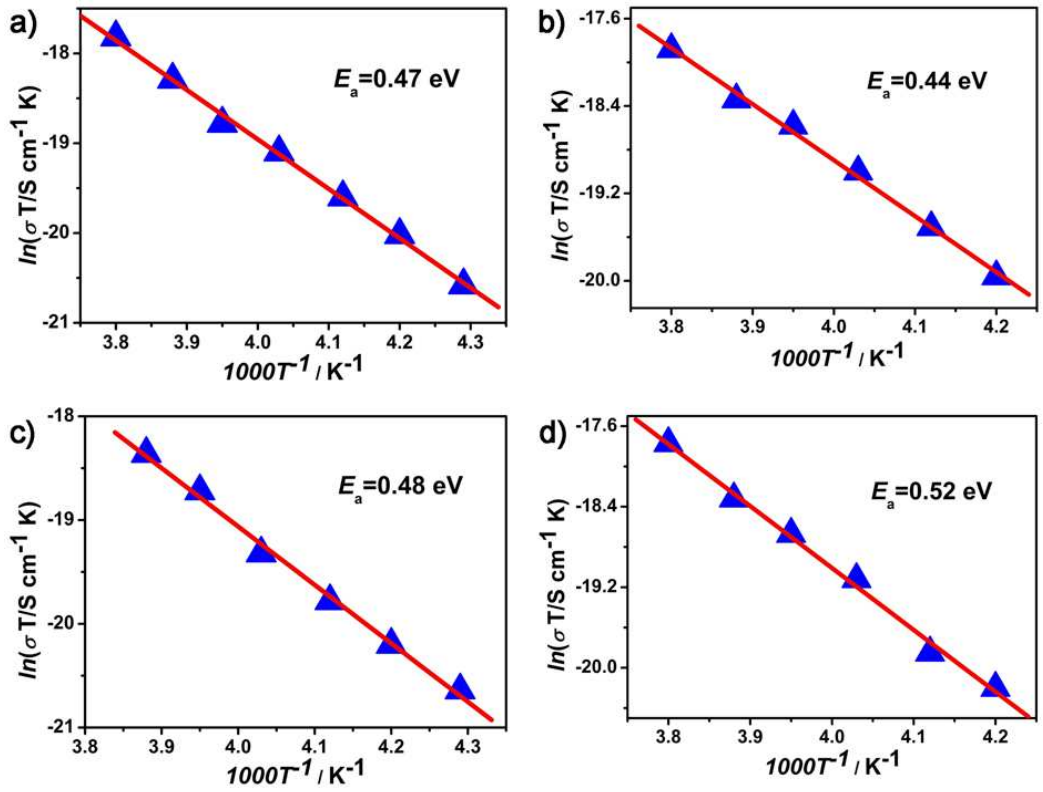

Cooling 1 (°C)	R1 R2 R3 (S^{-1})	$R'_{average}$ (S^{-1})	Fitting Parameter (Y=A+B*X)		
-10	1.91E8 1.99E8 2.58E8	2.16E8	Parameter	Value	Error
-15	3.44E8 3.54E8 3.55E8	3.51E8	A	3.06666	0.49493
-20	5.61E8 5.91E8 5.95E8	5.82E8	B	-5.50607	0.12245
-25	7.17E8 7.45E8 9.89E8	8.17E8			
-30	1.24E9 1.24E9 1.69E9	1.39E9	R_{fit}=-0.99877		
-35	2.03E9 2.15E9 2.30E9	2.16E9			
-40	3.59E9 3.96E9 3.97E9	3.84E9			

Heating 1 (°C)					
-35	1.88E9 1.99E9 2.22E9	2.03E9	Parameter	Value	Error
-30	1.21E9 1.23E9 1.33E9	1.26E9	A	1.61468	0.62984
-25	7.16E8 7.26E8 7.70E8	7.37E8	B	-5.12753	0.1575
-20	4.37E8 4.93E8 4.95E8	4.75E8			
-15	3.62E8 3.76E8 3.79E8	3.72E8	R_{fit}=-0.99812		
-10	2.02E8 2.38E8 2.47E8	2.29E8			
Cooling 2 (°C)					
-15	3.44E8 3.93E8 3.94E8	3.77E8	Parameter	Value	Error
-20	4.93E8 5.65E8 5.77E8	5.45E8	A	3.46936	0.77478
-25	1.04E9 1.07E9 9.5E8	1.02E9	B	-5.63286	0.18986
-30	1.48E9 1.74E9 1.76E9	1.66E9			
-35	2.29E9 2.67E9 2.74E9	2.57E9	R_{fit}=-0.99774		
-40	3.93E9 3.94E9 4.4E9	4.09E9			
Heating 2 (°C)					
-35	2.43E9 2.58E9 2.72E9	2.575E9	Parameter	Value	Error
-30	1.57E9 1.80E9 1.97E9	1.78E9	A	5.5857	0.86542
-25	7.78E8 8.20E8 8.92E8	8.3E8	B	-6.14863	0.21641
-20	4.88E8 5.14E8 5.60E8	5.21E8			
-15	3.38E8 3.74E8 3.75E8	3.62E8	R_{fit}=-0.99753		
-10	1.84E8 2.02E8 2.33E8	2.06E8			

Figure S52 Arrhenius plots of MIL-101-SO_3H for the every cooling-heating cycle (at subzero temperatures). (a) the first cooling cycle (-10--40 °C). (b) the first heating cycle (-35--10 °C). (c) the second cooling cycle (-15--40 °C). (d) the second heating cycle (-35--10 °C). The fitting line (red line) is shown to calculate the value of E_a.

Below: The table shows corresponding fitting parameters including R (the resistances from Nyquist plots, respectively), $R'_{average}$ (average resistance), A (intercept of fitting line), B (slope of fitting line) and R_{fit} (The closer the R value is to 1, the better the degree of fitting is).

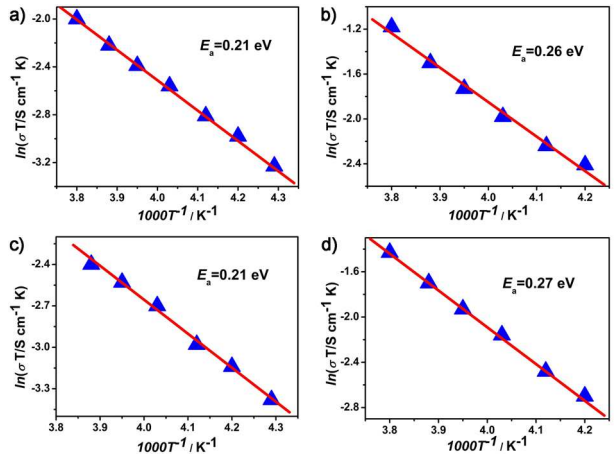

Cooling 1 (°C)	R1	R2	R3 (S^{-1})	$R'_{average}$ (S^{-1})	Fitting Parameter (Y=A+B*X)		
-10	27.568	32.483	33.168	31.073	Parameter	Value	Error
-15	37.870	38.061	42.35	39.427	A	7.37774	0.14392
-20	45.620	47.488	48.522	47.210	B	-2.47026	0.03561
-25	52.708	53.720	64.557	56.995			
-30	74.466	74.834	76.726	75.342	R_{fit}=-0.99948		
-35	89.123	92.110	93.768	91.667			
-40	100.045	119.51	139.53	119.695			
Heating 1 (°C)							
-35	51.055	51.911	52.381	51.78	Parameter	Value	Error
-30	37.257	42.865	48.255	42.79	A	10.4387	0.57938
-25	30.349	31.704	33.615	31.89	B	-3.07224	0.14488
-20	21.535	21.884	29.921	24.45			
-15	13.948	17.419	26.233	19.20	R_{fit}=-0.99558		
-10	12.384	12.995	15.601	13.66			
Cooling 2 (°C)							
-15	45.112	47.722	49.408	47.414	Parameter	Value	Error
-20	53.112	54.637	57.251	55	A	7.05895	0.32866
-25	62.918	63.112	71.574	65.868	B	-2.43088	0.08854
-30	85.64	90.704	91.949	89.431			
-35	104.19	112.09	113.72	110	R_{fit}=-0.99781		
-40	139.23	139.7	140.51	139.81			

Heating 2 (°C)					
-35	66.122 67.482 73.942	69.182	Parameter	Value	Error
-30	52.829 55.202 55.349	54.46	A	10.5922	0.1614
-25	37.121 37.673 40.19	38.328	B	-3.16944	0.04036
-20	25.075 30.23 34.125	29.81			
-15	20.375 23.748 26.227	23.45	R_{fit}=-0.99968		
-10	17.257 17.553 17.822	17.544			

Figure S53 Arrhenius plots of H_2SO_4@MIL-101-SO_3H (3M) for the every cooling-heating cycle (at subzero temperatures). (a) the first cooling cycle (-10--40 °C). (b) the first heating cycle (-35--10 °C). (c) the second cooling cycle (-15--40 °C). (d) the second heating cycle (-35--10 °C). The fitting line (red line) is shown to calculate the value of E_a.

Below: The table shows corresponding fitting parameters including R (the resistances from Nyquist plots, respectively), $R'_{average}$ (average resistance), A (intercept of fitting line), B (slope of fitting line) and R_{fit} (The closer the R value is to 1, the better the degree of fitting is).

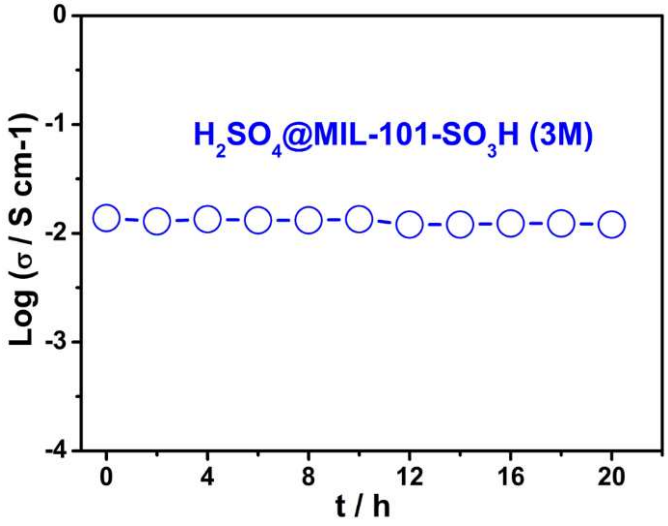

Figure S54 Time-dependent proton conductivity of H_2SO_4@MIL-101-SO_3H (3M) performed at -40 °C.

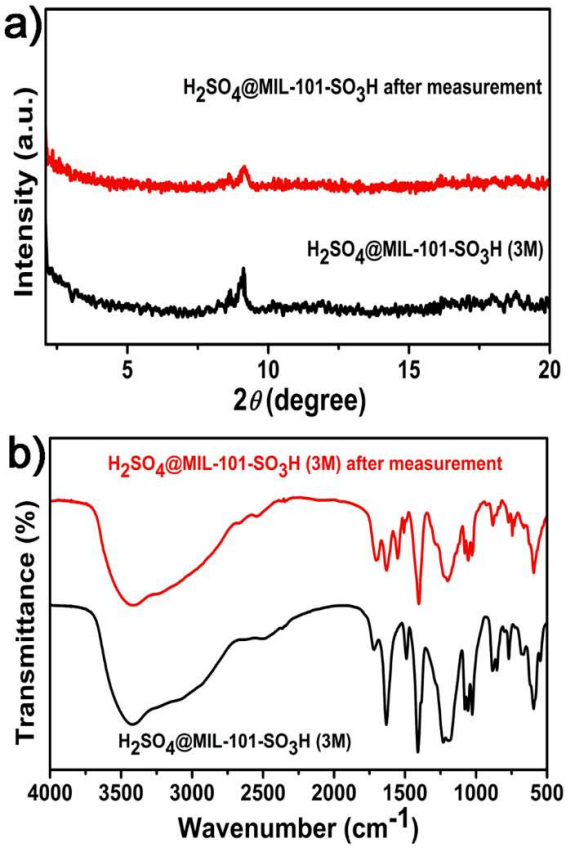

Figure S55 (a) PXRD patterns and (b) FT-IR spectra of as-synthesized H_2SO_4@MIL-101-SO_3H (3M) (black) and H_2SO_4@MIL-101-SO_3H (3M) undergoing time-dependent conductivity measurement (red)

.

Table S1. Comparison of proton conductivity of H_2SO_4@MIL-101-SO_3H (3M) with some other representative proton conductors measured under hydrous condition.

Compounds	**σ (S cm^{-1})**	**E_a (eV)**	**Reference**
H_2SO_4@MIL-101-SO_3H (3M) (powder)	3.55×10^{-1} (30°C, 90%RH)	0.39	This work
H_2SO_4@MIL-101-SO_3H (3M) (powder)	1.82 (70°C, 90%RH)	0.39	This work
H_2SO_4@MIL-101 (3M) (powder)	1.60×10^{-1} (30°C, 90%RH)	0.33	This work
H_2SO_4@MIL-101 (3M) (powder)	6.09×10^{-1} (70°C, 90%RH)	0.33	This work
MIL-101-SO_3H (powder)	1.68×10^{-5} (30°C, 90%RH)	0.27	This work
MIL-101-SO_3H (powder)	6.32×10^{-5} (70°C, 90%RH)	0.27	This work
Nafion (powder)	5×10^{-2} (30°C, 98%RH)	0.22	3

$Fe(ox)\cdot 2H_2O$ (powder)	3.23×10^{-3} (45°C, 98%RH)	0.37	4
PCMOF-3 (powder)	3.5×10^{-5} (25°C,98%RH)	0.17	5
$(NH_4)_4[MnCr_2(ox)_6]\cdot 4H_2O$ (powder)	1.7×10^{-3} (40°C, 96%RH)	0.23	6
$Fe(OH)(bdc\text{-}(COOH)_2)$ (powder)	7×10^{-6} (80°C, 95%RH)	0.21	7
$Cu_3Mo_5P_2$ (powder)	2.2×10^{-5} (28°C, 98%RH)	0.23	8
$\{NMe_3(CH_2COOH)\}[FeCr(ox)_3]\cdot nH_2O$ (powder)	0.8×10^{-4} (25°C, 65%RH)	/	9
$\{NEt_3(CH_2COOH)\}[MnCr(ox)_3]\cdot nH_2O$ (powder)	2×10^{-4} (25°C, 80%RH)	/	9
$\{NBu_3(CH_2COOH)\}[MnCr(ox)_3]\cdot nH_2O$ (powder)	5×10^{-6} (25°C, 90%RH)	/	9
$\{NBu_3(CH_2COOH)\}[FeCr(ox)_3]\cdot nH_2O$ (powder)	0.9×10^{-7} (25°C, 90%RH)	/	9
Ca-SBBA (powder)	8.58×10^{-6} (25°C, 98%RH)	0.23	10
Sr-SBBA (powder)	4.4×10^{-5} (25°C, 98%RH)	0.56	10
H_2SO_4@MIL-101 (2.7M) (powder)	1.0×10^{-2} (150°C, 0.13%RH)	/	11
In-IA-2D-1 (powder)	3.4×10^{-3} (27°C, 98%RH)	0.61	12
In-IA-2D-2 (powder)	4.2×10^{-4} (27°C, 98%RH)	0.48	12
PCMOF-5 (powder)	2.51×10^{-3} (60°C, 98%RH)	0.16	13
$\{H[Cu(Hbpdc(H_2O)_2]_2[PMo_{12}O_{40}]\cdot nH_2O\}_n$ (powder)	1.25×10^{-3} (100°C, 98%RH)	1.02	14
$\{H[Cu(Hbpdc(H_2O)_2]_2[PW_{12}O_{40}]\cdot nH_2O\}_n$ (powder)	156×10^{-3} (100°C, 98%RH)	1.02	14
$\{[Ca(D\text{-}Hpmpc)(H_2O)_2]\cdot 2HO_{0.5}\}_n$ (powder)	8.9×10^{-4} (60°C, 97%RH)	0.21	15
$\{H[Ni(Hbpdc)(H_2O)_2]_2[PW_{12}O_{40}]\cdot 8H_2O$ (powder)	1.35×10^{-3} (100°C, 98%RH)	1.01	16
$\{[H_3O][Cu_2(DSOA)(OH)(H_2O)]\cdot 9.5H_2O\}_n$ (powder)	1.9×10^{-3} (85°C, 98%RH)	1.04	17
PCMOF2½ (powder)	2.1×10^{-2} (85°C, 90%RH)	0.21	18
$\{[(Me_2NH_2)_3(SO_4)]_2[Zn(ox)_3]\}_n$ (powder)	4.2×10^{-2} (25°C, 98%RH)	0.12	19
EuL (powder)	1.6×10^{-5} (75°C, 97%RH)	0.91	20
DyL (powder)	1.33×10^{-5} (75°C, 97%RH)	0.87	20
HKUST-1 (powder)	1.08×10^{-8} (90°C, 70%RH)	0.69	21

NENU-3 (powder)	4.76×10^{-5} (90°C, 70%RH)	0.41	21
NENU-3-Ina (powder)	1.81×10^{-3} (90°C, 70%RH)	0.36	21
$(NH_4)_2(adp)[Zn_2(ox)_3]\cdot2H_2O$ (powder)	7×10^{-5} (25°C, 100%RH)	/	22
$(NH_4)_2(adp)[Zn_2(ox)_3]\cdot3H_2O$ (powder)	8×10^{-3} (25°C, 100%RH)	/	22
H^+@Ni_2(dobdc) pH=1.8 (powder)	2.2×10^{-2} (80°C, 95%RH)	0.12	23
$\{[Cu_3(L)_2(H_2O)_4][Cu(dmf)_4(SiW_{12}O_{40})]\cdot9H_2O$ (powder)	5.94×10^{-4} (100°C, 98%RH)	0.32	24
$[H_3O][CoLa(notp)(H_2O)_4]ClO_4\cdot3H_2O$ (powder)	4.24×10^{-5} (25°C, 98%RH)	0.28	25
$[Cu_3(u_3OH)(H_2O)_3(atz)_3]_3[P_2W_{18}O_{62}]\cdot14H_2O$ (powder)	4.4×10^{-6} (25°C, 97%RH)	/	26
$[Cu(H_2L)(DMF)_4]_n$ (powder)	3.46×10^{-3} (95°C, 95%RH)	0.68	27
$[CaL_{0.5}(DMF)_{2.5}]_n$ (powder)	1.27×10^{-5} (25°C, 95%RH)	0.17	27
$[CdL_{0.5}(DMF)_2]_n$ (powder)	2.49×10^{-7} (25°C, 95%RH)	0.59	27
$[Cd_2(btc)_2(H_2O)_2]_n\cdot n(H_2bmib)\cdot6n(H_2O)$ (powder)	5.4×10^{-5} (60°C, 95%RH)	0.62	28
$[Cd_4(cpip)_2(Hcpip)_2]_n\cdot n(H_2bmib)\cdot n(H_2O)$ (powder)	2.2×10^{-5} (60°C, 95%RH)	0.27	28
ZIF8 (powder)	4.6×10^{-4} (94°C, 98%RH)	/	29
PCMOF10 (powder)	3.55×10^{-2} (70°C, 95%RH)	0.4	30
$\{[Zn(C_{10}H_2O_8)_{0.5}(C_{10}S_2N_2H_8)]\cdot5H_2O]\}_n$ (powder)	2.55×10^{-7} (80°C, 95%RH)	0.96	31
$\{[Zn(C_{10}H_2O_8)_{0.5}(C_{10}S_2N_2H_8)]\cdot2H_2O]\}_n$ (powder)	4.39×10^{-4} (80°C,95%RH)	0.84	31
$Cu_4(L)_2(OH)_2(DMF)_2$ (powder)	7.4×10^{-4} (95°C, 95%RH)	1.32	32
UiO-66$(SO_3H)_2$ (powder)	8.4×10^{-2} (80°C, 90%RH)	0.32	33
UiO-66(Zr)-$(CO_2H)_2$ (powder)	2.3×10^{-3} (90°C, 95%RH)	0.17	34
$[Cu_3(BTC)_2(H_2O)_3]_4[SiW_{11}Mo^vO_{40}](C_4H_{12}N_5)\cdot30H_2O$ (powder)	6.37×10^{-8} (25°C, 97%RH)	/	35
VNU-15 (powder)	2.90×10^{-2} (95°C, 60%RH)	0.22	36
MFM-500 (Ni) (powder)	4.5×10^{-4} (25°C, 98%RH)	0.43	37

Im = Imidazole, ox = oxalate, PCMOF-3 = $Zn_3(L)(H_2O)_2\cdot2H_2O$ (L = 1,3,5-benzenetriphosphonate), H_2bdc = 1,4-benzenedicarboxylic acid, In-IA-2D-1 = $[In(IA)_2\{(CH_3)_2NH_2\}(H_2O)_2]$ In-IA-2D-2 = $[In(IA)_2\{(CH_3)_2NH_2\}(DMF)]$ (IA = isophthalic

acid), PCMOF-5 = $LaH_5L(H_2O)_4$ (L = Benzene-1,2,4,5-tetramethylenephosphonic acid), H_2bpd = 2,2′-bipyridyl-3,3′-dicarboxylic acid, D-H_2pmpc = D-1-(phosphonomethyl)piperdine-3-carboxylic acid, Na_2H_2DSOA = disodium-2,2′-disulfonate-4,4′-oxydibenzoic acid, adp = adipic acid, $dobdc^{4-}$ = 2,5-dioxido-1,4-benzenedicarboxylate, notpH_6=$C_9H_{18}N_3(PO_3H_2)_3$, Hatz = 3-amino-1,2,4,triazolate, H_3btc = 1,3,5-benzenetricarboxylic acid, H_3cpip = 5-(4-carboxyphenoxy)isophthalic acid, PCMOF10 = $Mg_2(H_2O)_4(H_2L)\cdot H_2O$ (H_6L = 2,5-dicarboxy-1,4-benzenediphosphonic acid), BTC = 1,3,5-benzenetricarboxylate, VNU-15 = $Fe_4(BDC)_2(NDC)(SO_4)_4(DMA)_4$ (BDC = benzene-1,4-dicarboxylate, NDC = naphthalene-2,6-dicarboxylate), MFM-500(Ni) = $[M_3(H_3L)_2(H_2O)_9(C_2H_6SO)_3]$ (M=Ni, H_6L = benzene-1,3,5-p-phenylphosphonic acid)

Table S2. Comparison of proton conductivities measured at -40°C between our work and reported proton conductors.

Compounds	**σ (S cm^{-1})**	***E*$_a$ (eV)**	**Reference**
Im@Td-PPI (powder)	2.23×10^{-6}	0.30	38
Im@Td-PNDI (powder)	4.58×10^{-7}	0.33	38
FJU-31@Hq (powder)	3.24×10^{-6}	0.18	39
FJU-31@Ch (powder)	1.17×10^{-6}	0.29	39
MIL-101-SO_3H (powder)	2.68×10^{-10}	0.47	This work
H_2SO_4@MIL-101 (3M) (powder)	1.06×10^{-3}	0.17	This work
H_2SO_4@MIL-101-SO_3H (3M) (powder)	0.92×10^{-2}	0.21	This work

Table S3. Conductivity (σ) values of H_2SO_4@MIL-101-SO_3H (3M) in the range of -10 to -40°C.

Temperature (°C)	σ (S cm^{-1})
-10	3.54×10^{-2}
-15	2.79×10^{-2}
-20	2.33×10^{-2}
-25	1.93×10^{-2}
-30	1.46×10^{-2}
-35	1.20×10^{-2}
-40	0.92×10^{-2}

Table S4. Variation of proton conductivities with different concentrations of H_2SO_4 in MIL-101 at 30°C, 90%RH and -40°C respectively.

Compounds	S/Cr	H_2SO_4/MIL-101	σ (S cm^{-1}) (30°C, 90%RH)	σ (S cm^{-1}) (-40°C)
H_2SO_4@MIL-101 (1M)	1.01	3.03	7.55×10^{-2}	1.75×10^{-4}
H_2SO_4@MIL-101 (2M)	1.59	4.77	1.04×10^{-1}	2.80×10^{-4}
H_2SO_4@MIL-101 (3M)	2.10	5.64	1.60×10^{-1}	1.06×10^{-3}

S/Cr: atomic ratio of S and Cr, H_2SO_4/MIL-101: the number of H_2SO_4 molecules per MIL-101 formula unit that calculated from EDS results.

Table S5. Variation of proton conductivities with different concentrations of H_2SO_4 in MIL-101-SO_3H at 30°C, 90%RH and -40°C respectively.

Compounds	S/Cr	H_2SO_4/MIL-101-SO_3H	σ (S cm^{-1}) (30°C, 90%RH)	σ (S cm^{-1}) (-40°C)
H_2SO_4@MIL-101-SO_3H(1M)	0.85	2.55	7.88×10^{-3}	2.12×10^{-3}
H_2SO_4@MIL-101-SO_3H(2M)	0.95	2.85	1.85×10^{-2}	4.18×10^{-3}
H_2SO_4@MIL-101-SO_3H(3M)	1.31	3.93	3.55×10^{-1}	0.92×10^{-2}

S/Cr: atomic ratio of S and Cr, H_2SO_4/MIL-101-SO_3H: the number of H_2SO_4 molecules per MIL-101-SO_3H formula unit that calculated from EDS results.

Table S6. The E_a values of different temperature ranges for H_2SO_4@MIL-101 (3M), MIL-101-SO_3H and H_2SO_4@MIL-101-SO_3H (3M).

Compounds	E_a (eV) (30~70°C)	E_a (eV) (-40~-10°C)
H_2SO_4@MIL-101 (3M)	0.33	0.17
MIL-101-SO_3H	0.27	0.47
H_2SO_4@MIL-101-SO_3H (3M)	0.39	0.21

3. Reference:

(1) Ferey, G.; Mellot-Draznieks, C.; Serre, C.; Millange, F.; Dutour, J.; Surble, S.; Margiolaki, I. A chromium terephthalate-based solid with unusually large pore volumes and surface area. *Science* **2005,** *309,* 2040-2042.

(2) Zhou, Y.-X.; Chen, Y.-Z.; Hu, Y.; Huang, G.; Yu, S.-H.; Jiang, H.-L. MIL-101-SO_3H: A Highly Efficient Brønsted Acid Catalyst for Heterogeneous Alcoholysis of Epoxides under Ambient Conditions. *Chem. Eur. J.* **2014,** *20,* 14976-14980.

(3) Slade, R. C. T.; Hardwick, A.; Dickens, P. G. Investigation of H^+ motion in NAFION film by pulsed 1H NMR and A.C. conductivity measurements. *Solid State Ionics* **1983,** *9,* 1093-1098.

(4) Yamada, T.; Sadakiyo, M.; Kitagawa, H. High Proton Conductivity of One-Dimensional Ferrous Oxalate Dihydrate. *J. Am. Chem. Soc.* **2009,** *131,* 3144-3145.

(5) Taylor, J. M.; Mah, R. K.; Moudrakovski, I. L.; Ratcliffe, C. I.; Vaidhyanathan, R.; Shimizu, G. K. H. Facile Proton Conduction via Ordered Water Molecules in a Phosphonate Metal−Organic Framework. *J. Am. Chem. Soc.* **2010,** *132,* 14055-14057.

(6) Pardo, E.; Train, C.; Gontard, G.; Boubekeur, K.; Fabelo, O.; Liu, H.; Dkhil, B.; Lloret, F.; Nakagawa, K.; Verdaguer, M et al. High Proton Conduction in a Chiral Ferromagnetic Metal–Organic Quartz-like Framework. *J. Am. Chem. Soc.* **2011,** *133,* 15328-15331.

(7) Shigematsu, A.; Yamada, T.; Kitagawa, H. Wide Control of Proton Conductivity in Porous Coordination Polymers. *J. Am. Chem. Soc.* **2011,** *133,* 2034-2036.

(8) Dey, C.; Kundu, T.; Banerjee, R. Reversible phase transformation in proton conducting Strandberg-type POM based metal organic material. *Chem. Commun.* **2012,** *48,* 266-268.

(9) Sadakiyo, M.; Ōkawa, H.; Shigematsu, A.; Ohba, M.; Yamada, T.; Kitagawa, H. Promotion of Low-Humidity Proton Conduction by Controlling Hydrophilicity in Layered Metal–Organic Frameworks. *J. Am. Chem. Soc.* **2012,** *134,* 5472-5475.

(10) Kundu, T.; Sahoo, S. C.; Banerjee, R. Alkali earth metal (Ca, Sr, Ba) based thermostable metal-organic frameworks (MOFs) for proton conduction. *Chem. Commun.* **2012,** *48,* 4998-5000.

(11) Ponomareva, V. G.; Kovalenko, K. A.; Chupakhin, A. P.; Dybtsev, D. N.; Shutova, E. S.; Fedin, V. P. Imparting High Proton Conductivity to a Metal–Organic Framework Material by Controlled Acid Impregnation. *J. Am. Chem. Soc.* **2012,** *134,* 15640-15643.

(12) Panda, T.; Kundu, T.; Banerjee, R. Structural isomerism leading to variable proton conductivity in indium(iii) isophthalic acid based frameworks. *Chem. Commun.* **2013,** *49,* 6197-6199.

(13) Taylor, J. M.; Dawson, K. W.; Shimizu, G. K. H. A Water-Stable Metal–Organic Framework with Highly Acidic Pores for Proton-Conducting Applications. *J. Am. Chem. Soc.* **2013,** *135,* 1193-1196.

(14) Wei, M.; Wang, X.; Duan, X. Crystal Structures and Proton Conductivities of a MOF and Two POM–MOF Composites Based on CuII Ions and 2,2′-Bipyridyl-3,3′-dicarboxylic Acid. *Chem. Eur. J.* **2013,** *19,* 1607-1616.

(15) Liang, X.; Zhang, F.; Feng, W.; Zou, X.; Zhao, C.; Na, H.; Liu, C.; Sun, F.; Zhu, G. From metal-organic framework (MOF) to MOF-polymer composite membrane: enhancement of low-humidity proton conductivity. *Chem. Sci.* **2013,** *4,* 983-992.

(16) Wei, M.; Wang, X.; Sun, J.; Duan, X. A 3D POM–MOF composite based on Ni(II) ion and 2,2′-bipyridyl-3,3′-dicarboxylic acid: Crystal structure and proton conductivity. *J. Solid State Chem.* **2013,** *202,* 200-206.

(17) Dong, X.-Y.; Wang, R.; Li, J.-B.; Zang, S.-Q.; Hou, H.-W.; Mak, T. C. W. A tetranuclear $Cu_4(\mu_3\text{-}OH)_2$-based metal-organic framework (MOF) with sulfonate-carboxylate ligands for proton conduction. *Chem. Commun.* **2013,** *49,* 10590-10592.

(18) Kim, S.; Dawson, K. W.; Gelfand, B. S.; Taylor, J. M.; Shimizu, G. K. H. Enhancing Proton Conduction in a Metal–Organic Framework by Isomorphous Ligand Replacement. *J. Am. Chem. Soc.* **2013,** *135,* 963-966.

(19) Nagarkar, S. S.; Unni, S. M.; Sharma, A.; Kurungot, S.; Ghosh, S. K. Two-in-One: Inherent Anhydrous and Water-Assisted High Proton Conduction in a 3D Metal–Organic Framework. *Angew. Chem., Int. Ed.* **2014,** *53,* 2638-2642.

(20) Zhu, M.; Hao, Z.-M.; Song, X.-Z.; Meng, X.; Zhao, S.-N.; Song, S.-Y.; Zhang, H.-J. A new type of double-chain based 3D lanthanide(iii) metal-organic framework demonstrating proton conduction and tunable emission. *Chem. Commun.* **2014,** *50,* 1912-1914.

(21) Liu, Y.; Yang, X.; Miao, J.; Tang, Q.; Liu, S.; Shi, Z.; Liu, S. Polyoxometalate-functionalized metal-organic frameworks with improved water retention and uniform proton-conducting pathways in three orthogonal directions. *Chem. Commun.* **2014,** *50,* 10023-10026.

(22) Sadakiyo, M.; Yamada, T.; Honda, K.; Matsui, H.; Kitagawa, H. Control of Crystalline Proton-Conducting Pathways by Water-Induced Transformations of Hydrogen-Bonding Networks in a Metal–Organic Framework. *J. Am. Chem. Soc.* **2014,** *136,* 7701-7707.

(23) Phang, W. J.; Lee, W. R.; Yoo, K.; Ryu, D. W.; Kim, B.; Hong, C. S. pH-Dependent Proton Conducting Behavior in a Metal–Organic Framework Material. *Angew. Chem., Int. Ed.* **2014,** *53,* 8383-8387.

(24) Wei, M.-L.; Sun, J.-J.; Duan, X.-Y. A Complex Based on a CuII–Schiff-Base Complex and POM-MOF Chain: Synthesis, Structure and Proton Conductivity. *Eur. J. Inorg. Chem.* **2014,** *2014,* 345-351.

(25) Bao, S.-S.; Otsubo, K.; Taylor, J. M.; Jiang, Z.; Zheng, L.-M.; Kitagawa, H. Enhancing Proton Conduction in 2D Co–La Coordination Frameworks by Solid-State Phase Transition. *J. Am. Chem. Soc.* **2014,** *136,* 9292-9295.

(26) Jiao, Y.-Q.; Zang, H.-Y.; Wang, X.-L.; Zhou, E.-L.; Song, B.-Q.; Wang, C.-G.; Shao, K.-Z.; Su, Z.-M. Self-assembled arrays of polyoxometalate-based metal-organic nanotubes for proton conduction and magnetism. *Chem. Commun.* **2015,** *51,* 11313-11316.

(27) Zhao, S.-N.; Song, X.-Z.; Zhu, M.; Meng, X.; Wu, L.-L.; Song, S.-Y.; Wang, C.; Zhang, H.-J. Assembly of three coordination polymers based on a sulfonic-carboxylic ligand showing high proton conductivity. *Dalton. Trans.* **2015,** *44,* 948-954.

(28) Li, X.; Sun, X.; Li, X.; Fu, Z.; Su, Y.; Xu, G. Porous Cadmium(II) Anionic Metal–Organic Frameworks Based on Aromatic Tricarboxylate Ligands: Encapsulation of Protonated Flexible Bis(2-methylimidazolyl) Ligands and Proton Conductivity. *Cryst. Growth Des.* **2015,** *15,* 4543-4548.

(29) Barbosa, P.; Rosero-Navarro, N. C.; Shi, F.-N.; Figueiredo, F. M. L. Protonic Conductivity of Nanocrystalline Zeolitic Imidazolate Framework 8. *Electrochimica Acta* **2015,** *153,* 19-27.

(30) Ramaswamy, P.; Wong, N. E.; Gelfand, B. S.; Shimizu, G. K. H. A Water Stable Magnesium MOF That Conducts Protons over 10^{-2} S cm^{-1}. *J. Am. Chem. Soc.* **2015,** *137,* 7640-7643.

(31) Sanda, S.; Biswas, S.; Konar, S. Study of Proton Conductivity of a 2D Flexible MOF and a 1D Coordination Polymer at Higher Temperature. *Inorg. Chem.* **2015,** *54,* 1218-1222.

(32) Meng, X.; Song, S.-Y.; Song, X.-Z.; Zhu, M.; Zhao, S.-N.; Wu, L.-L.; Zhang, H.-J. A tetranuclear copper cluster-based MOF with sulfonate-carboxylate ligands exhibiting high proton conduction properties. *Chem. Commun.* **2015,** *51,* 8150-8152.

(33) Phang, W. J.; Jo, H.; Lee, W. R.; Song, J. H.; Yoo, K.; Kim, B.; Hong, C. S. Superprotonic Conductivity of a UiO-66 Framework Functionalized with Sulfonic Acid Groups by Facile Postsynthetic Oxidation. *Angew. Chem., Int. Ed.* **2015,** *54,* 5142-5146.

(34) Borges, D. D.; Devautour-Vinot, S.; Jobic, H.; Ollivier, J.; Nouar, F.; Semino, R.; Devic, T.; Serre, C.; Paesani, F.; Maurin, G. Proton Transport in a Highly Conductive Porous Zirconium-Based Metal–Organic Framework: Molecular Insight. *Angew. Chem., Int. Ed.* **2016,** *128,* 3987-3992.

(35) Li, C.; Sun, M.; Xu, L.; Wang, Y.; Huang, J. The first heteropoly blue-embedded metal-organic framework: crystal structure, magnetic property and proton conductivity. *CrystEngComm.* **2016,** *18,* 596-600.

(36) Tu, T. N.; Phan, N. Q.; Vu, T. T.; Nguyen, H. L.; Cordova, K. E.; Furukawa, H. High proton conductivity at low relative humidity in an anionic Fe-based metal-organic framework. *J. Mater. Chem. A.* **2016,** *4,* 3638-3641.

(37) Pili, S.; Argent, S. P.; Morris, C. G.; Rought, P.; García-Sakai, V.; Silverwood, I. P.; Easun, T. L.; Li, M.; Warren, M. R.; Schröder, M et al. Proton Conduction in a Phosphonate-Based Metal–Organic Framework Mediated by Intrinsic "Free Diffusion inside a Sphere". *J. Am. Chem. Soc.* **2016,** *138,* 6352-6355.

(38) Ye, Y.; Zhang, L.; Peng, Q.; Wang, G.-E.; Shen, Y.; Li, Z.; Wang, L.; Ma, X.; Chen, Q.-H.; Xiang, S et al. High Anhydrous Proton Conductivity of Imidazole-Loaded Mesoporous Polyimides over a Wide Range from Subzero to Moderate Temperature. *J. Am. Chem. Soc.* **2015,** *137,* 913-918.

(39) Ye, Y.; Wu, X.; Yao, Z.; Wu, L.; Cai, Z.; Wang, L.; Ma, X.; Chen, Q.-H.; Zhang, Z.; Xiang, S. Metal-organic frameworks with a large breathing effect to host hydroxyl compounds for high anhydrous proton conductivity over a wide temperature range from subzero to 125 °C. *J. Mater. Chem. A.* **2016**, *4,* 4062-4070.